Acknowledgments

This work was supported by a Grant-in-Aid from the Ministry of Education, Science, Sports, and Culture of Japan (25461343 to K. Hotta, 23791027 to A. K., and 23701082 to T. K.).

Disclosure Statement

None of the authors have any potential conflicts of interest associated with this research.

Supplementary Table 1 Genotypic characteristics of the subjects

SNP ID	Chr	Position (Build 36.3)	Nearby gene	allele1/ allele2	Risk allele	Genotype		Risk allele frequency		HWE *P*-value	
						Men	Women	Men	Women	Men	Women
rs1514175	1	74,764,232	*TNNI3K*	A/G	A	429/190/14	562/207/20	0.83	0.84	0.18	0.86
rs1555543	1	96,717,385	*PTBP2*	A/C	C	16/162/453	13/209/566	0.85	0.85	0.74	0.20
rs713586	2	25,011,512	*ADCY3*	C/T	C	154/337/142	243/368/178	0.51	0.54	0.10	0.088
rs2943650	2	226,814,165	*IRS1*	C/T	T	9/121/503	11/119/659	0.89	0.91	0.58	**0.040**
rs2112347	5	75,050,998	*POC5*	G/T	T	195/314/118	248/367/168	0.44	0.45	0.67	0.14
rs206936	6	34,410,847	*NUDT3*	A/G	G	110/303/220	150/377/262	0.59	0.57	0.75	0.49
rs10968576	9	28,404,339	*LINGO2*	A/G	G	392/209/28	519/240/28	0.21	0.19	0.98	0.97
rs4929949	11	8,561,169	*STK33*	C/T	C	101/333/196	160/372/255	0.42	0.44	**0.040**	0.25
rs4771122	13	26,918,180	*MTIF3*	A/G	G	375/229/30	446/302/41	0.23	0.24	0.51	0.27
rs534870	13	79,857,208	*SPRY2*	A/G	A	186/329/117	256/399/134	0.55	0.58	0.18	0.31
rs2241423	15	65,873,892	*MAP2K5*	A/G	G	245/299/87	310/370/108	0.37	0.37	0.78	0.89
rs2287019	19	50,894,012	*QPCTL*	C/T	C	425/186/22	499/258/30	0.82	0.80	0.77	0.64
rs3810291	19	52,260,843	*ZC3H4*	A/G	A	52/219/360	47/269/471	0.26	0.23	**0.026**	0.30

Chr, chromosome; HWE, Hardy–Weinberg equilibrium. Number in bold indicate *P*-value <0.05.

Supplementary Table 2 The association of the 13 SNPs with metabolic traits

SNP ID	Nearby gene	FPG (mg/dL)		Insulin (μU/mL)		HOMA-IR		T. Chol. (mg/dL)	
		β (s.e.)	*P*-value	β (s.e.)	*P*-value	β (s.e.)	*P*-value	β (s.e.)	*P*-value
rs1514175	*TNNI3K*	0.000 (0.005)	0.95	0.017 (0.016)	0.29	0.013 (0.018)	0.49	-0.118 (1.944)	0.95
rs1555543	*PTBP2*	-0.002 (0.005)	0.67	0.027 (0.016)	0.095	0.024 (0.018)	0.20	0.193 (2.004)	0.92
rs713586	*ADCY3*	-0.008 (0.004)	**0.032**	0.003 (0.012)	0.77	-0.004 (0.013)	0.78	0.223 (1.419)	0.87
rs2943650	*IRS1*	0.006 (0.006)	0.33	-0.024 (0.019)	0.20	-0.020 (0.022)	0.34	1.879 (2.328)	0.42
rs2112347	*POC5*	0.001 (0.004)	0.75	0.003 (0.012)	0.80	0.003 (0.013)	0.84	-3.160 (1.419)	**0.026**
rs206936	*NUDT3*	0.003 (0.004)	0.40	-0.011 (0.012)	0.33	-0.009 (0.013)	0.50	-1.147 (1.427)	0.42
rs10968576	*LINGO2*	0.002 (0.005)	0.62	-0.026 (0.015)	0.072	-0.027 (0.017)	0.10	5.881 (1.779)	**0.00097**
rs4929949	*STK33*	0.004 (0.004)	0.31	0.003 (0.012)	0.77	0.006 (0.014)	0.63	1.056 (1.451)	0.47
rs4771122	*MTIF3*	-0.009 (0.005)	0.053	-0.024 (0.014)	0.083	-0.035 (0.016)	**0.028**	-1.415 (1.700)	0.41
rs534870	*SPRY2*	0.002 (0.004)	0.58	0.002 (0.012)	0.88	0.005 (0.014)	0.73	0.336 (1.468)	0.82
rs2241423	*MAP2K5*	0.005 (0.004)	0.22	0.004 (0.012)	0.73	0.008 (0.014)	0.57	1.492 (1.479)	0.31
rs2287019	*QPCTL*	0.001 (0.005)	0.81	0.002 (0.015)	0.90	0.001 (0.017)	0.94	2.855 (1.806)	0.11
rs3810291	*ZC3H4*	0.000 (0.004)	0.95	0.000 (0.013)	0.98	-0.001 (0.015)	0.93	0.537 (1.616)	0.74

SNP ID	Nearby gene	Triglycerides (mg/dL)		HDL-C (mg/dL)		SBP (mmHg)		DBP (mmHg)	
		β (s.e.)	*P*-value	β (s.e.)	*P*-value	β (s.e.)	*P*-value	β (s.e.)	*P*-value
rs1514175	*TNNI3K*	-0.003 (0.012)	0.80	0.723 (0.753)	0.34	-0.343 (0.905)	0.70	-0.209 (0.629)	0.74
rs1555543	*PTBP2*	-0.007 (0.012)	0.54	0.015 (0.774)	0.98	-0.590 (0.943)	0.53	-0.488 (0.653)	0.45
rs713586	*ADCY3*	0.008 (0.009)	0.33	-0.769 (0.550)	0.16	-1.243 (0.661)	0.060	-0.547 (0.460)	0.23
rs2943650	*IRS1*	-0.020 (0.014)	0.16	1.036 (0.901)	0.25	-0.205 (1.085)	0.85	-0.180 (0.755)	0.81
rs2112347	*POC5*	-0.005 (0.009)	0.55	-0.859 (0.548)	0.12	-0.107 (0.667)	0.87	-0.373 (0.463)	0.42
rs206936	*NUDT3*	0.006 (0.009)	0.49	-0.272 (0.554)	0.62	0.694 (0.665)	0.30	0.265 (0.462)	0.57
rs10968576	*LINGO2*	0.021 (0.011)	0.056	-0.385 (0.690)	0.58	0.835 (0.823)	0.31	0.154 (0.573)	0.79
rs4929949	*STK33*	0.020 (0.009)	**0.021**	-0.648 (0.562)	0.25	-0.235 (0.673)	0.73	-0.126 (0.468)	0.79
rs4771122	*MTIF3*	-0.005 (0.010)	0.65	-0.179 (0.661)	0.79	0.426 (0.785)	0.59	0.313 (0.546)	0.57
rs534870	*SPRY2*	0.023 (0.009)	**0.0094**	-1.865 (0.567)	**0.0010**	0.628 (0.680)	0.36	0.351 (0.473)	0.46
rs2241423	*MAP2K5*	0.001 (0.009)	0.95	-0.050 (0.572)	0.93	-0.410 (0.693)	0.56	-0.146 (0.482)	0.76
rs2287019	*QPCTL*	-0.006 (0.011)	0.58	-0.105 (0.702)	0.88	0.142 (0.849)	0.87	0.074 (0.590)	0.90
rs3810291	*ZC3H4*	0.013 (0.010)	0.17	-0.028 (0.628)	0.96	0.781 (0.751)	0.30	0.626 (0.517)	0.23

Abbreviations: DBP, diastolic blood pressure; FPG, fasting plasma glucose; HDL-C, high density lipoprotein cholesterol; HOMA-IR; homeostasis model assessment-insulin resistance index; SBP, systolic blood pressure; SNP, single-nucleotide polymorphism; T. Chol., total cholesterol. HOMA-IR was assessed as fasting insulin (μU/mL) × fasting plasma glucose/405. Data were derived from a linear regression analysis. The values of FPG, insulin, HOMA-IR, and triglycerides were logarithmically transformed. Each metabolic phenotype was adjusted for age, gender, and logarithmically transformed BMI. Numbers in bold indicate *P*-value <0.05.

References

1. Carr DB, Utzschneider KM, Hull RL, Kodama K, Retzlaff BM, et al. (2004) Intra-abdominal fat is a major determinant of the National Cholesterol Education Program Adult Treatment Panel III criteria for the metabolic syndrome. *Diabetes* 53: 2087-2094.
2. Matsuzawa Y (2006) Therapy insight: adipocytokines in metabolic syndrome and related cardiovascular disease. *Nat Clin Pract Cardiovasc Med* 3: 35-42.
3. Hotta K, Funahashi T, Bodkin NL, Ortmeyer HK, Arita Y, et al. (2001) Circulating concentrations of the adipocyte protein adiponectin are decreased in parallel with reduced insulin sensitivity during the progression to type 2 diabetes in rhesus monkeys. *Diabetes* 50: 1126-1133.
4. Selby JV, Newman B, Quesenberry CP Jr, Fabsitz RR, Carmelli D, et al. (1990) Genetic and behavioral influences on body fat distribution. *Int J Obes* 14: 593-602.
5. Rose KM, Newman B, Mayer-Davis EJ, Selby JV (1998) Genetic and behavioral determinants of waist-hip ratio and waist circumference in women twins. *Obes Res* 6: 383-392.
6. Mills GW, Avery PJ, McCarthy MI, Hattersley AT, Levy JC, et al. (2004) Heritability estimates for beta cell function and features of the insulin resistance syndrome in UK families with an increased susceptibility to type 2 diabetes. *Diabetologia* 47: 732-738.
7. Souren NY, Paulussen AD, Loos RJ, Gielen M, Beunen G, et al. (2007) Anthropometry, carbohydrate and lipid metabolism in the East Flanders Prospective Twin Survey: heritabilities. *Diabetologia* 50: 2107-2116.
8. Mastuzawa Y (2005) Metabolic syndrome – definition and diagnostic criteria in Japan. *J Atheroscler Thromb* 12: 301.
9. Arai H, Yamamoto A, Matsuzawa Y, Saito Y, Yamada N, et al. (2006) Prevalence of metabolic syndrome in the general Japanese population in 2000. *J Atheroscler Thromb* 13: 202-208.
10. Lindgren CM, Heid IM, Randall JC, Lamina C, Steinthorsdottir V, et al. (2009) Genome-wide association scan meta-analysis identifies three loci influencing adiposity and fat distribution. *PLoS Genet* 5: e1000508.
11. Heard-Costa NL, Zillikens MC, Monda KL, Garcia M, Launer LJ, et al. (2009) NRXN3 is a novel locus for waist circumference: a genome-wide association study from the CHARGE Consortium. *PLoS Genet* 5: e1000539.
12. Heid IM, Jackson AU, Randall JC, Winkler TW, Qi L, et al. (2010) Meta-analysis identifies 13 new loci associated with waist-hip ratio and reveals sexual dimorphism in the genetic basis of fat distribution. *Nat Genet* 42: 949-960.
13. Fox CS, Liu Y, White CC, Feitosa M, Smith AV, et al. (2012) Genome-wide association for abdominal subcutaneous and visceral adipose reveals a novel locus for visceral fat in women. *PLoS Genet* 8: e1002695.
14. Hotta K, Nakamura M, Nakamura T, Matsuo T, Nakata Y, et al. (2010) Polymorphisms in NRXN3, TFAP2B, MSRA, LYPLAL1, FTO and MC4R and their effect on visceral fat area in the Japanese population. *J Hum Genet* 55: 738-742.
15. Hotta K, Kitamoto A, Kitamoto T, Mizusawa S, Teranishi H, et al. (2012) Association between type 2 diabetes genetic susceptibility loci and visceral and subcutaneous fat area as determined by computed tomography. *J Hum Genet* 57: 305-310.
16. Hotta K, Kitamoto A, Kitamoto T, Mizusawa S, Teranishi H, et al. (2013) Replication study of 15 recently published loci for body fat distribution in the Japanese population. *J Atheroscler Thromb* 20: 336-350.
17. Thorleifsson G, Walters GB, Gudbjartsson DF, Steinthorsdottir V, Sulem P, et al. (2009) Genome-wide association yields new sequence variants at seven loci that associate with measures of obesity. *Nat Genet* 41: 18-24.
18. Willer CJ, Speliotes EK, Loos RJ, Li S, Lindgren CM, et al. (2009) Six new loci associated with body mass index highlight a neuronal influence on body weight regulation. *Nat Genet* 41: 25-34.
19. Meyre D, Delplanque J, Chèvre JC, Lecoeur C, Lobbens S, et al. (2009) Genome-wide association study for early-onset and morbid adult obesity identifies three new risk loci in European populations. *Nat Genet* 41: 157-159.
20. Hotta K, Kitamoto T, Kitamoto A, Mizusawa S, Matsuo T, et al. (2011) Computed tomography analysis of the association between SH2B1 rs7498665 single-nucleotide polymorphism and visceral fat area. *J Hum Genet* 56: 716-719.
21. Speliotes EK, Willer CJ, Berndt SI, Monda KL, Thorleifsson G, et al. (2010) Association analyses of 249,796 individuals reveal 18 new loci associated with body mass index. *Nat Genet* 42: 937-938.
22. Kilpeläinen TO, Zillikens MC, Stančáková A, Finucane FM, Ried JS, et al. (2011) Genetic variation near IRS1 associates with reduced adiposity and an impaired metabolic profile. *Nat Genet* 43: 753-760.
23. Examination Committee of Criteria for 'Obesity Disease' in Japan; Japan Society for the Study of Obesity (2002) New criteria for 'obesity disease' in Japan. *Circ J* 66: 987-992.
24. Yoshizumi T, Nakamura T, Yamane M, Islam AH, Menju M, et al. (1999) Abdominal fat: standardized technique for measurement at CT. *Radiology* 211: 283-286.
25. Ohnishi Y, Tanaka T, Ozaki K, Yamada R, Suzuki H, et al. (2001) A high-throughput SNP typing system for

genome-wide association studies. *J Hum Genet* 46: 471-477.
26. Nielsen DM, Ehm MG, Weir BS (1998) Detecting marker-disease association by testing for Hardy–Weinberg disequilibrium at a marker locus. *Am J Hum Genet* 63: 1531-1540.
27. Kotani K, Tokunaga K, Fujioka S, Kobatake T, Keno Y, et al. (1994) Sexual dimorphism of age-related changes in whole-body fat distribution in the obese. *Int J Obes Relat Metab Disord* 18: 207-202.
28. Matsushita Y, Nakagawa T, Yamamoto S, Takahashi Y, Yokoyama T, et al. (2010) Associations of visceral and subcutaneous fat areas with the prevalence of metabolic risk factor clustering in 6,292 Japanese individuals: the Hitachi Health Study. *Diabetes Care* 33: 2117-2119.
29. Fujioka S, Matsuzawa Y, Tokunaga K, Tarui S (1987) Contribution of intra-abdominal fat accumulation to the impairment of glucose and lipid metabolism in human obesity. *Metabolism* 36: 54-59.
30. Burgdorf KS, Gjesing AP, Grarup N, Justesen JM, Sandholt CH, et al. (2012) Association studies of novel obesity-related gene variants with quantitative metabolic phenotypes in a population-based sample of 6,039 Danish individuals. *Diabetologia* 55: 105-113.
31. Hong KW, Oh B (2012) Recapitulation of genome-wide association studies on body mass index in the Korean population. *Int J Obes* 36: 1127-1130.
32. Zillikens MC, Yazdanpanah M, Pardo LM, Rivadeneira F, Aulchenko YS, et al. (2008) Sex-specific genetic effects influence variation in body composition. *Diabetologia* 51: 2233-2241.
33. Hotta K, Kitamoto A, Kitamoto T, Mizusawa S, Teranishi H, et al. (2012) Genetic variations in the CYP17A1 and NT5C2 genes are associated with a reduction in visceral and subcutaneous fat areas in Japanese women. *J Hum Genet* 57: 46-51.
34. Lonetti A, Szijgyarto Z, Bosch D, Loss O, Azevedo C, et al. (2011) Identification of an evolutionarily conserved family of inorganic polyphosphate endopolyphosphatases. *J Biol Chem* 286: 31966-31974.
35. Shears SB (2009) Diphosphoinositol polyphosphates: metabolic messengers? *Mol Pharmacol* 76: 236-252.
36. Chakraborty A, Koldobskiy MA, Bello NT, Maxwell M, Potter JJ, et al. (2010) Inositol pyrophosphates inhibit Akt signaling, thereby regulating insulin sensitivity and weight gain. *Cell* 143: 897-910.

Original Article
CLINICAL TRIALS: BEHAVIOR, PHARMACOTHERAPY, DEVICES, SURGERY

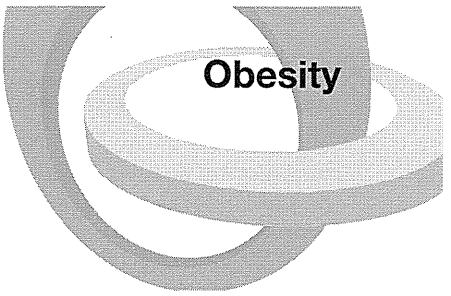

Early Changes of Abdominal Adiposity Detected with Weekly Dual Bioelectrical Impedance Analysis during Calorie Restriction

Midori Ida[1], Masakazu Hirata[1], Shinji Odori[1], Eisaku Mori[1], Eri Kondo[1], Junji Fujikura[1], Toru Kusakabe[1], Ken Ebihara[1], Kiminori Hosoda[1,2] and Kazuwa Nakao[1]

Objective: To elucidate early change of intra-abdominal fat in response to calorie restriction in patients with obesity by weekly evaluation using a dual bioelectrical impedance analysis (Dual BIA) instrument.
Design and Methods: For 67 Japanese patients with obesity, diabetes, or metabolic syndrome, intra-abdominal fat area (IAFA), initially with both Dual BIA and computed tomography (CT), and in subsequent weeks of calorie restriction, with Dual BIA were measured.
Results: IAFA by Dual BIA (Dual BIA-IAFA) correlated well with IAFA by CT (CT-IAFA) in obese patients ($r = 0.821$, $P < .0001$, $n = 67$). Ten males and 9 females (age 49.0 ± 14.4 years, BMI 33.2 ± 7.3 kg/m^2) lost more than 5% of baseline body weight (BW) in 3 weeks, and their Dual BIA-IAFA, BW, and WC decreased by 18.9%, 5.3%, and 3.8%, respectively ($P < .05$, ANCOVA).
Conclusion: Dual BIA instrument could detect the weekly change of Dual BIA-IAFA under calorie restriction in obese patients and demonstrated a substantially larger change of IAFA compared with changes of BW and WC in early weeks. This observation corroborates the significance of evaluating IAFA as a biomarker for obesity, and indicates the clinical usefulness of the Dual BIA instrument.

Obesity (2013) **21**, E350-E353. doi:10.1002/oby.20300

Introduction

Abdominal adiposity is associated with development of obesity and metabolic abnormalities in obesity-related diseases (1-3). The adipose tissue distribution has been quantitatively evaluated by computed tomography (CT) (4) or magnetic resonance imaging (MRI) (5), and intra-abdominal fat area (IAFA) is used as a clinical parameter of abdominal adiposity (6). Although waist circumference (WC) is casually employed to evaluate abdominal adiposity (7), WC is known to reflect both the intra-abdominal and the subcutaneous abdominal adiposity. In addition, the correlation of WC with intra-abdominal adiposity is influenced by age and sex as shown in epidemiological studies (5). Thus, WC does not necessarily provide the precise information about abdominal fat distribution. Therefore, a new practical method for detecting early change in abdominal adiposity is needed to elucidate its consequence during acute phase of calorie restriction in obesity treatment (8). There have been a few proposals of methods (9,10) that assess IAFA as alternatives to CT (4) or MRI (5). However, there has been no report on clinical application of these methods analyzing the weekly change of IAFA during calorie restriction. We have developed the dual bioelectrical impedance analysis (Dual BIA) instrument that can determine IAFA by measuring truncal impedance and surface impedance at the abdomen separately, each of which reflects the truncal adiposity and the subcutaneous adiposity respectively (11-13). The Dual BIA instrument has been optimized with aims at robustness for use in a wide range of human variation by analyzing the size of effect that each parameter, such as age and gender, can have on the calculation outcomes utilizing information technology (11-13). In this study, we report on application of the Dual BIA instrument to compare the weekly change in IAFA and body weight (BW) of obese patients with the metabolic syndrome or diabetes mellitus resulting from calorie restriction.

Methods

Dual BIA method and instrumentation

Dual BIA instrument calculates the cross-sectional area of intra-abdominal fat at the level of umbilicus based on the measurement of electrical potentials resulting from applying small electrical currents in two different body space. Principles of IAFA determination by Dual BIA instrument have been described previously (11-13) in detail. Briefly, the Dual BIA instrument consists of bioelectrical impedance

[1] Department of Medicine and Clinical Science, Kyoto University Graduate School of Medicine, Sakyo-ku, Kyoto, Japan. Correspondence: Masakazu Hirata (mhirata@kuhp.kyoto-u.ac.jp) [2] Department of Human Health Science, Kyoto University Graduate School of Medicine, Sakyo-ku, Kyoto, 606-8507, Japan

Disclosure: The authors declared no conflict of interest.
Funding agencies: This work was supported in part by research grants from the Ministry of Education, Culture, Sports, Science and Technology of Japan including Grant in Aid for Scientific Research on Innovative Areas (Research in a proposed research area) "Molecular Basis and Disorders of Control of Appetite and Fat Accumulation", the Ministry of Health, Labour and Welfare of Japan, the Takeda Medical Research Foundation, the Smoking Research Foundation, Suzuken Memorial Foundation, Japan Foundation of Applied Enzymology, Novo Nordisk Insulin Research Award, Lilly Education and Research Grant Office.
Received: 8 May 2012 **Accepted:** 25 November 2012 **Published online 2 January 2013. doi:10.1002/oby.20300**

component that measures truncal and surface impedance of the body, and a device that measures physical size of the abdomen. The two sets of electrodes are for limb and truncal placement. The limb electrodes consist of four clip-on electrodes placed on wrists and ankles. The truncal electrodes are eight pairs of electrodes 6 cm apart longitudinally that are fixed to a belt where four pairs each for front and back are positioned at an equal inter-electrode distance. The belt is adjustable so that the electrodes are positioned centered on mid-sagittal line at the level of umbilicus in supine position. The truncal impedance is measured by applying electrical currents between upper and lower limb leads and reading voltage from the electrodes around the abdominal circumference. The surface impedance is measured by applying and reading voltage from the abdominal circumferential electrodes. IAFA by Dual BIA (Dual BIA-IAFA) is calculated as follows.

$$\text{Dual BIA} - \text{IAFA} = \alpha_1 A + \alpha_2 B^2 - \alpha_3 \left(A^2 + B^2\right)^{1/2} Z_s - \alpha_4 / Z_t + \varepsilon \quad (1)$$

A: abdominal antero-posterior diameter, B: abdominal transverse diameter, Z_s: surface impedance, Z_t: truncal impedance, ε: residual constant.

There was a good agreement of Dual BIA-IAFA and IAFA measured by CT (CT-IAFA) with the correlation coefficient of 0.888 ($n = 98$, $P < .001$) (13).

Patient selection

The study was performed according to the protocol approved by Kyoto University Medical Ethics Review Board (no. 080116). The patient gave a written consent to participate in this study which took place at the endocrinology and metabolism ward of Kyoto University Hospital. We collected data from 67 Japanese patients (36 males and 31 females; mean ± SD age, 54.7 ± 14.7 years, BMI 29.3 ± 6.5 kg/m^2) with obesity ($n = 56$), diabetes mellitus ($n = 45$), or the metabolic syndrome ($n = 38$) who were hospitalized for calorie restriction therapy or diet education, and had measurement of IAFA by both Dual BIA method and CT method at the start of calorie restriction. Obesity was diagnosed as BMI 25.0, and metabolic syndrome was diagnosed according to 2005 Japanese criteria of metabolic syndrome (14). Average daily calorie intake was 1437.3 ± 201.4 kcal/day (19.3 ± 4.3 kcal/ideal BW). Out of 67 patients, 35 patients could be followed for longer than 3 weeks, while the other patients were discharged earlier after examination of complications and diet and lifestyle education. Total daily energy was varied individually during hospitalization based on consultation between the patient, a dietician, and a physician. Out of 35 patients who had their Dual BIA-IAFA monitored every week for at least 3 weeks (four times), 19 patients lost more than 5% of baseline BW, and were included in the analysis of weekly change in Dual BIA-IAFA, WC, and BW during weight reduction.

Measurement of Dual BIA, CT, and anthropometric parameters

Dual BIA-IAFA was measured every week in the morning before breakfast depending on individual patient's treatment schedule (Figure 1A). Abdominal CT was performed for calculation of CT-IAFA within 7 days before the initial Dual BIA-IAFA measurement. CT-IAFA was calculated at umbilical level by the software, Virtual Place Lexus (AZE of Japan, Ltd). BW was measured to the nearest 0.1 kg in the morning of the Dual BIA-IAFA measurement.

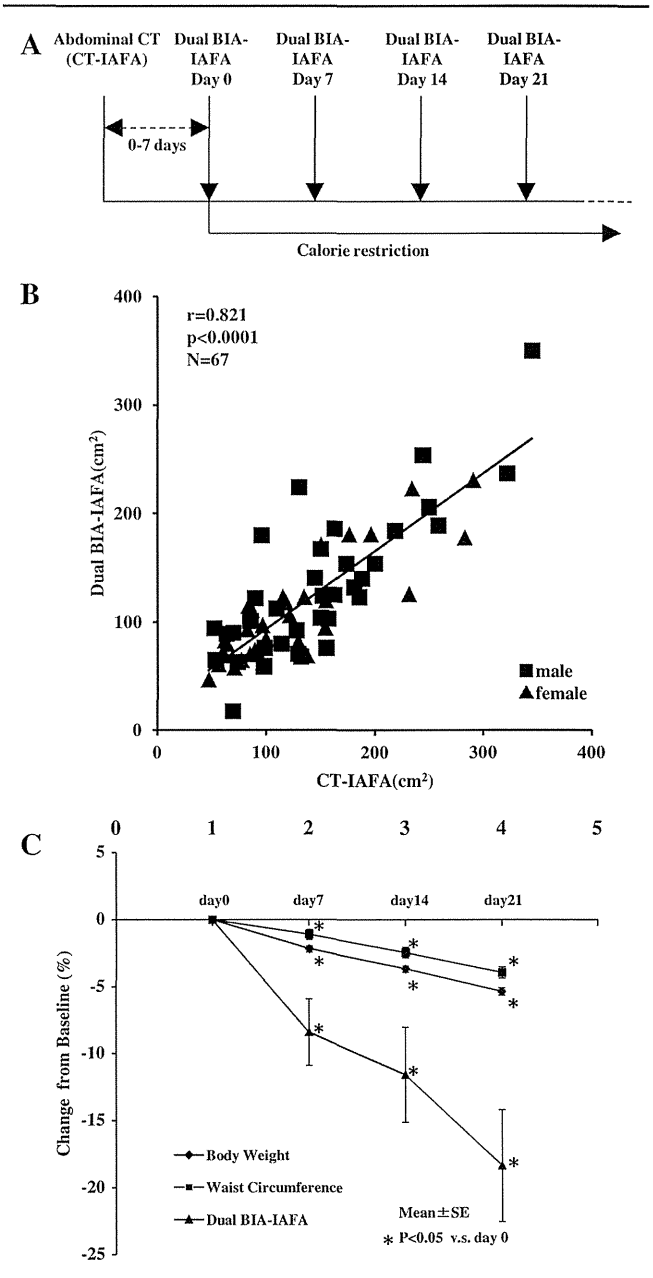

FIGURE 1 A: Diagram of IAFA assessment schedule during the calorie restriction. Patients started fixed calorie diet within 7 days of taking the abdominal CT image. Dual BIA-IAFA assessment took place in the morning before meal every week. CT imaging took place either in the morning or in the afternoon. **B**: Correlation between CT-IAFA and BIA-IAFA in 67 patients who were with obesity-related disorders. Square symbols: male, Triangle symbols: female. $r = 0.821$, $P < .001$ by Pearson's analysis. **C**: Weekly change of Dual BIA-IAFA plotted along with BW and WC during weight loss. Nineteen patients who underwent the calorie restriction and had abdominal CT examined at baseline were monitored for their anthropometric parameters and Dual BIA-IAFA weekly for at least 3 weeks. They lost more than 5% of BW during the period. Size of the change from baseline values (mean ± SE) is expressed as %. *$P < .05$ by Student's paired t-test.

WC was measured at the level of the umbilicus to the nearest 0.1 cm in the standing position at the end of expiration while breathing gently at the time of Dual BIA measurement.

Statistical methods

Correlation between values obtained by Dual BIA and CT were evaluated using Pearson's correlation analysis. Weekly values of Dual BIA-IAFA, BW, and WC were compared with the baseline values of day 0 by Student's paired *t*-test. Analysis of covariance was applied for comparison of Dual BIA-IAFA, BW, and WC at week 3.

Results

In 67 patients with obesity and related conditions, Dual BIA-IAFA correlated well with CT-IAFA ($r = 0.821$, $P < .0001$) (Figure 1B).

Thirty-five (17 males and 18 females) out of 67 patients were monitored with Dual BIA for longer than 3 weeks, and 19 (10 males and 9 females) out of 35 patients achieved weight loss of more than 5% of the initial BW. In order to elucidate the change in IAFA during weight loss, Dual BIA-IAFA, BW, and WC of the 19 patients were analyzed. Baseline characteristics of the 19 patients were (mean ± SD); age, 49.0 ± 14.4 years, height 163.0 ± 10.5 cm, BMI 33.2 ± 7.3 kg/m^2, and CT-IAFA 143.6 ± 47.4 cm^2. BW, WC, and Dual BIA-IAFA at baseline and at week 3 were: 89.2 ± 26.2 kg and 84.5 ± 25.1 kg, 110.6 ± 14.1 cm and 106.0 ± 14.2 cm, and 150.4 ± 73.7 cm^2 and 124.3 ± 70.3 cm^2, respectively.

Figure 1C shows the weekly change of Dual BIA-IAFA, BW, and WC in 19 patients whose BW decreased more than 5% during the 3 weeks of monitoring. Dual BIA-IAFA, BW and WC showed a significant reduction after 1 week during the calorie restriction compared with the baseline values ($P < .05$). Dual BIA-IAFA decreased every week for the initial 3 weeks and the average reduction in Dual BIA-IAFA was 18.9%, which was larger than in BW (5.3%) and WC (3.8%) (ANCOVA, $P < .05$).

Discussion

The present study demonstrates that the weekly change in IAFA can be detected with the Dual BIA instrument during the calorie restriction. Due to the practical limitations such as instrumentation and cost, CT and MRI are unsuitable for weekly monitoring of change in IAFA. There is also a problem of X-ray exposure in CT scanning. Consequently, it has been impractical to monitor IAFA weekly or frequently, in clinical follow-up period with CT or MRI. There have been several attempts to evaluate the IAFA by BIA (9-13). They include calculation from whole body impedance and from measuring abdominal impedance by the electrodes placed on the abdomen (9,10). Some of the estimates of IAFA incorporate gender and age of the subject in order to attain high correlation with CT (9,10). In contrast, Dual BIA, which is a method that is not dependent on external variables, such as gender or age, had shown a good correlation between Dual BIA-IAFA and CT-IAFA (11-13). In the present study, we confirmed the good correlation of Dual BIA-IAFA and CT-IAFA in obese patients. The correlation coefficient for the Dual BIA-IAFA and CT-IAFA was 0.821 ($n = 67$) with our subjects whose average BMI was 29.3. This indicates that Dual BIA produced reliable measurements with obesity patients and the result was comparable to the correlation coefficient of 0.888 obtained with subjects whose average BMI was around 25 (13). It must be noted that CT-IAFA and Dual BIA-IAFA was not measured on the same day in the present study, unlike the previous report in which Dual BIA- and CT-IAFA was taken on the same day (13), and therefore direct comparison has its limitations. By applying Dual BIA to monitoring the weekly change of individual body component during the calorie restriction, we could detect the characteristic change of IAFA. The significant decrease in Dual BIA-IAFA, BW, and WC at week 1 supports the suitability of selecting 5% of BW change at week 3 as a criterion for including in weekly analysis of these parameters.

On average, IAFA showed a larger reduction than BW and WC during the initial 3 weeks of calorie restriction. The rapid response of intra-abdominal adipose tissue to calorie restriction has been suggested in an ultrasonography study that examined a portion of peritoneal fat thickness (15). The larger decrease of Dual BIA-IAFA observed is also in agreement with a study which showed larger reduction in IAFA evaluated with MRI than that of BW up to 12 weeks on very low calorie diet (16). Together with these results, the present study established that the intra-abdominal fat decreases rapidly in the initial period of calorie restriction by measuring Dual BIA-IAFA, and demonstrates the usefulness of monitoring the change in IAFA during the treatment of obesity and its related disorders.

Weakness of our study is that its design was not of a prospective weight reduction where every participant was prescribed daily calorie that could produce predetermined level of weight loss within the study period. Instead we selected participants that had their weight decreased by at least 5% in order to illustrate the change in abdominal adiposity on weekly basis. It is also of note that the BW and Dual BIA-IAFA at week 1 may be affected by salt restriction and loss of body water that is observed early in calorie restriction. Because of the small sample size, the observed change in Dual BIA-IAFA could be larger than actual change. It also depends on the precision of the instrument. In a separate population, the coefficient of variation was 7.6% (Ida, M. manuscript in preparation).

In conclusion, the present study demonstrated that Dual BIA instrument can be used to measure IAFA in obese patients, allows frequent measurement, and is useful for detecting the early change in IAFA during calorie restriction. Information thus obtained along with other changes in metabolic parameters will be indispensable for understanding the role of abdominal adiposity, and especially useful as a diagnostic marker for monitoring obesity and its related disorders (1). In addition, the instrument's safety and convenience could be suitable for large population studies.O

Acknowledgments

Authors thank all the volunteers who took part in the study, and Research and Development Department of Omron Healthcare Corporation for use of the Dual BIA instrument.

References

1. Matsuzawa Y. The role of fat topology in the risk of disease. *Int J Obes* 2008;32: S83-S92.

2. Miyawaki T, Hirata M, Moriyama K, et al. Metabolic syndrome in Japanese diagnosed with visceral fat measurement by computed tomography. *Proc Jpn Acad Ser B* 2005;81:471-479.
3. Després JP, Lemieux I. Abdominal obesity and metabolic syndrome. *Nature* 2006; 444:881-887.
4. Ferland M, Després JP, Trembly A, et al. Assessment of adipose tissue distribution by computed axial tomography in obese women: association with body density and anthropometric measurements. *Br J Nutr* 1989;61:139-148.
5. Kuk JL, Lee S, Heymsfield SB, Ross R. Waist circumference and abdominal adipose tissue distribution: influence of age and sex. *Am J Clin Nutr* 2005;81: 1330-1334.
6. Cornier MA, Després JP, Davis N, et al. A scientific statement from the American Heart Association. *Circulation* 2011;124:1996-2019.
7. Miyawaki T, Abe M, Yahata K, Kajiyama N, Katsuma H, Saito N. Contribution of visceral fat accumulation to the risk factors for atherosclerosis in non-obese Japanese. *Intern Med* 2004;43:1138-1144.
8. Isbess JM, Tamboli RA, Hansen EN, et al. The importance of caloric restriction in the early improvements in insulin sensitivity after Roux-en Y gastric bypass surgery. *Diabetes Care* 2010;33:1438-1442.
9. Ryo M, Maeda K, Onda T, et al. A new simple method for the measurement of visceral fat accumulation by bioelectrical impedance. *Diabetes Care* 2005;8:451-453.
10. Nagai M, Komiya H, Mori Y, Ohta T, Kasahara Y, Ikeda Y. Development of a new method for estimating visceral fat area with multi-frequency bioelectrical impedance. *Tohoku J Exp Med* 2008;214:105-112.
11. Shiga T, Oshima Y, Kanai H, Hirata M, Hosoda K, Nakao K. *A simple measurement method of visceral fat accumulation by bioelectrical impedance analysis*, In: *IFMBE Proceedings*, Vol. 17/14: 13th International Conference on Electrical Bioimpedance and the 8th Conference on Electrical Impedance Tomography; Scharfetter H, et al., eds., Springer-Verlag; 2007, pp 687-690.Available at: http://link.springer.com/chapter/10.1007%2F978-3-540-73841-1_177?LI=true.
12. Yoneda M, Tasaki H, Tsuchiya N, et al. A study of bioelectrical impedance analysis methods for practical visceral fat estimation. In: IEEE International Conference on Granular Computing (GCR 2007), Lin TY, et al., eds., IEEE Computer Society Press; 2007, pp 622-627. Available at: http://ieeexplore.ieee.org/xpl/login.jsp?tp=&arnumber=4403174&url=http%3A%2F%2Fieeexplore.ieee.org%2Fxpls%2Fabs_all.jsp%3Farnumber%3D4403174.
13. Shiga T, Hamaguchi T, Oshima Y, et al. *A new simple measurement system of visceral fat accumulation by bioelectrical impedance analysis.* In *IFMBE Proceedings* Vol. 25/7: World Congress on Medical Physics and Biomedical Engineering, Döossel O, et al., eds., Springer-Verlag; 2009, pp 338-341.
14. Matsuzawa Y. Metabolic syndrome—definition and diagnostic criteria in Japan. *J Atheroscler Thromb* 2005;12:301.
15. Li Y, Bujo H, Takahashi K, et al. Visceral Fat: higher responsiveness of fat mass and gene expression to calorie restriction than subcutaneous fat. *Exp Biol Med (Maywood)* 2003;228:1118-1123.
16. Colles SL, Dixon JB, Marks P, et al. Preoperative weight loss with a very-low-energy diet: quantitation of changes in liver and abdominal fat by serial imaging. *Am J Clin Nutr* 2006;84:304-311.

Am J Physiol Endocrinol Metab 305: E140–E148, 2013.
First published May 7, 2013; doi:10.1152/ajpendo.00112.2013.

Overexpression of intraislet ghrelin enhances β-cell proliferation after streptozotocin-induced β-cell injury in mice

Mika Bando,[1,3] Hiroshi Iwakura,[1] Hiroyuki Ariyasu,[1] Hiroyuki Koyama,[2] Kiminori Hosoda,[2,3] Souichi Adachi,[3] Kazuwa Nakao,[2] Kenji Kangawa,[4] and Takashi Akamizu[1,5]

[1]*Ghrelin Research Project, Translational Research Center, Kyoto University Hospital, Kyoto University Graduate School of Medicine, Kyoto, Japan;* [2]*Department of Medicine and Clinical Science, Endocrinology and Metabolism, Kyoto University Graduate School of Medicine, Kyoto, Japan;* [3]*Department of Human Health Sciences, Kyoto University Graduate School of Medicine, Kyoto, Japan;* [4]*National Cerebral and Cardiovascular Center Research Institute, Osaka, Japan,* [5]*The First Department of Medicine, Wakayama Medical University, Wakayama, Japan*

Submitted 28 February 2013; accepted in final form 2 May 2013

Bando M, Iwakura H, Ariyasu H, Koyama H, Hosoda K, Adachi S, Nakao K, Kangawa K, Akamizu T. Overexpression of intraislet ghrelin enhances β-cell proliferation after streptozotocin-induced β-cell injury in mice. *Am J Physiol Endocrinol Metab* 305: E140–E148, 2013. First published May 7, 2013; doi:10.1152/ajpendo.00112.2013.— Previously, we reported that exogenous administration of ghrelin ameliorates glucose metabolism in a neonate streptozotocin (STZ)-induced diabetic rat model through enhancement of β-cell proliferation. However, it was not clear whether the observed β-cell proliferation was a direct or indirect effect (e.g., via orexigenic or growth hormone-stimulated pathways) of ghrelin activity. Here, we aimed to investigate whether ghrelin directly impacts β-cell proliferation after STZ-induced injury in mice. Seven-week-old male rat insulin II promoter-ghrelin internal ribosomal sequence ghrelin *O*-acyltransferase transgenic (RIP-GG Tg) mice, which have elevated pancreatic ghrelin levels, but only minor changes in plasma ghrelin levels when fed a medium-chain triglyceride-rich diet, were treated with STZ. Then, serum insulin, pancreatic insulin mRNA expression, and islet histology were evaluated. We found that the serum insulin levels, but not blood glucose levels, of RIP-GG Tg mice were significantly ameliorated 14 days post-STZ treatment. Pancreatic insulin mRNA expression was significantly elevated in RIP-GG Tg mice, and β-cell numbers in islets were increased. Furthermore, the number of phospho-histone $H3^+$ or $Ki67^+$ proliferating β-cells was significantly elevated in RIP-GG Tg mice, whereas the apoptotic indexes within the islets, as determined by TUNEL assay, were not changed. These results indicate that ghrelin can directly stimulate β-cell proliferation in vivo after β-cell injury even without its orexigenic or GH-stimulating activities, although it did not have enough impact to normalize the glucose tolerance in adult mice.

ghrelin; β-cell; diabetes; streptozotocin

DECREASED INSULIN SECRETION is one of the major features of diabetes. Insulin is produced in pancreatic islets by β-cells, whose numbers are reduced or eliminated during the pathology of the disease. Autoimmune-mediated destruction of β-cells causes type 1 diabetes, and a decrease in β-cell mass is also noted in patients with type 2 diabetes (5). Accordingly, a substantial effort has been made toward preventing or reversing β-cell degradation. One approach has been to find hormones or growth factors that impact proliferation or survival after β-cell injury. Several hormones, including growth hormone (GH) (22), prolactin (11), and glucagon-like peptide-1 (GLP-1) (11), have been suggested to stimulate β-cell proliferation in cell lines or animal models. Although these hormones have not yet been tested in the clinic, this approach may lead to the development of a new class of antidiabetic drugs.

Ghrelin is a 28-amino acid stomach-derived peptide hormone bearing a unique acyl modification on the third Ser residue, which is essential for binding to its receptor (18). We (13) previously reported that exogenous ghrelin administration prevents the development of diabetes at the adult stage of a rat neonate streptozotocin (STZ) model. In that study, we observed increased numbers of phospho-histone $H3^+$/$insulin^+$ cells in the islets of ghrelin-treated rats, suggesting that ghrelin had enhanced β-cell proliferation. However, it was not clear whether that was a direct or indirect effect of ghrelin treatment. Because ghrelin strongly stimulates GH secretion (18, 27) and food intake (20, 25), we could not rule out the possibilities that elevated GH or nutritional status may have affected β-cell proliferation (6).

Here, we directly examined the effects of ghrelin on β-cells after STZ treatment by using a recently developed rat insulin II promoter-ghrelin internal ribosomal sequence ghrelin *O*-acyltransferase (GOAT) transgenic (RIP-GG Tg) mice, in which ghrelin and GOAT genes are overexpressed in pancreatic β-cells under the control of the rat insulin II promoter (2). Compared with control mice, RIP-GG Tg mice display an ~16-fold increase in pancreatic ghrelin concentrations but no change in plasma ghrelin levels when fed a medium-chain triglyceride-rich diet (MCTD) (2). The aim of this study was to determine whether ghrelin directly stimulated the proliferation of β-cells after STZ-induced injury.

MATERIALS AND METHODS

RIP-GG Tg mice. RIP-GG Tg mice were generated as reported previously (2). In this study, we used male heterozygous Tg mice along with their non-Tg littermates as controls. Animals were maintained on a 12:12-h light-dark cycle and fed a standard diet (SD; CE-2, 352 kcal/100 g; Japan CLEA, Tokyo, Japan) or an MCTD containing 45% Dermol M5 (C8:60%, C10:40%; Research Diet, New Brunswick, NJ) as indicated. RIP-GG Tg mice showed elevated pancreatic ghrelin only when they were on MCTD, presumably due to the lack of machinery providing octanoyl acid for acylation in β-cells (2). RIP-GG Tg mice have normal glucose tolerance and insulin secretion in the absence of STZ (2). All experimental procedures were approved by the Kyoto University Graduate School of Medicine Committee on Animal Research.

STZ treatment. Seven-week-old male mice were randomly assigned to vehicle or STZ groups. STZ (100 mg/kg body wt in 100 mM citrate buffer, pH 4.5; Sigma-Aldrich, St. Louis, MO) or vehicle alone was injected after overnight fasting.

Address for reprint requests and other correspondence: H. Iwakura, 54 Shogoin Kawahara-cho, Sakyo-ku, Kyoto 606-8507, Japan (e-mail: hiwaku@kuhp.kyoto-u.ac.jp).

Blood glucose levels were determined by the glucose oxidase method using a Glutest sensor (Sanwa Kagaku, Kyoto, Japan), and serum insulin levels were determined using an Ultrasensitive Plus Mouse Insulin kit or a High-Range Speedy Mouse Insulin kit (Morinaga, Yokohama, Japan).

Real-time quantitative RT-PCR. Total RNA was extracted from pancreata using an RNeasy Protect minikit (Qiagen, Hilden, Germany). Reverse transcription (RT) was performed using a high-capacity cDNA reverse transcription kit (Applied Biosystems, Foster City, CA). Real-time quantitative PCR was performed on an ABI PRISM 7500 Sequence Detection System (Applied Biosystems) using the following primers and TaqMan probes: mouse ghrelin, sense 5′-GCATGCTCGGATGGACATG-3′, antisense 5′-TGGTGGCTTCTTGGATTCCT-3′; TaqMan probe 5′-AGCCCAGAGCACCAGAAAGCCCA-3′; mouse insulin 1, sense 5′-CAGCTATAATCAGAGACCATCAGCAA-3′, antisense 5′-GGGTAGGAAGTGCACCAACAG-3′; TaqMan probe 5′-CAGGTCATTGTTTCAAC-3′; mouse Pdx1, sense 5′-CAAAGCTCACGCGTGGAA-3′, antisense 5′-TGTAGGCAGTACGGGTCCTCTT-3′; TaqMan probe 5′-AGGAGGTGCTTACAC-3′; mouse GHS-R, sense 5′-CTGCTCACCGTGATGGTATG-3′, antisense 5′-CAGCAGAGGATGAAAGCAAA-3′, with Power SybrGreen. Data were normalized to the 18S rRNA content in each sample.

Pancreatic insulin concentration. To measure pancreatic insulin concentration, pancreata were obtained from the mice under the ether anesthesia and homogenized in acid-ethanol. The supernatants were used for assay after centrifugation.

Immunohistochemistry. Formalin-fixed, paraffin-embedded tissue sections were immunostained using the avidin-biotin peroxidase complex method (Vectastain ABC Elite Kit; Vector Laboratories, Burlingame, CA) as described previously (14). Serial sections (5 μm) were incubated with anti-insulin antibody (1:500; DAKO, Glostrup, Denmark). Counterstaining was performed with Mayer's hematoxylin.

Quantitative evaluations of insulin$^+$ areas were performed using WinROOF (Mitani, Fukui, Japan). For each pancreas, insulin$^+$ areas and islets were evaluated using five sections spaced more than 40 μm apart. The number of insulin$^+$ cells within an islet was counted in five sections spaced more than 40 μm apart. The relative volume of insulin$^+$ cells was determined by calculating the ratio between the area occupied by insulin$^+$ cells and the area encompassed by islet cells.

β-Cell proliferation. To detect β-cell proliferation, pancreatic tissue sections were double-stained to detect both phospho-histone H3 (Ser^{10}) or Ki67 and insulin. First, the immunoreactivity of the anti-phospho-histone H3 (Ser^{10}) antibody (1:50; Cell Signaling Technology, Beverly, MA) or anti-Ki67 antibody (1:25; BD Pharmingen, Franklin Lakes, NJ) was detected using a Vectastain ABC Elite kit with a DAB (DAKO) substrate. Then, the sections were incubated with anti-insulin antibody (1:500, DAKO), which was visualized with VECTOR VIP (Vector Laboratories). Quantitation of β-cell proliferation was performed by counting phospho-histone H3$^+$ or Ki67$^+$/insulin$^+$ cells using five sections spaced more than 40 μm apart. The relative number of phospho-histone H3$^+$ or Ki67$^+$ cells was determined by calculating the ratio between the numbers of phospho-histone H3$^+$ or Ki67$^+$ cells and insulin$^+$ cells.

Apoptosis. Apoptotic cells were detected using the terminal deoxynucleotidyltransferase-mediated dUTP nick-end labeling (TUNEL) assay (ApoMark apoptosis detection kit; Exalpha Biologicals, Maynard, MA). Quantitation of apoptotic cells was performed by counting TUNEL$^+$ cells within islets using five sections spaced more than 40 μm apart. The number of TUNEL$^+$ cells was presented as the number of TUNEL$^+$ cells/area of necrotic β-cells.

To detect apoptotic cells with DNA not yet fragmented, pancreatic tissue sections were stained with anti-cleaved caspase-3 (Asp175) antibody (1:300; Cell Signaling Technology, Beverly, MA). Quantitation of apoptotic cells was performed by counting cleaved caspase-3$^+$ cells within islets using five sections spaced more than 40 μm apart. The number of cleaved caspase-3$^+$ cells was presented as the number of cleaved caspase-3$^+$ cells/area of necrotic β-cells.

Statistical analyses. All values are expressed as means ± SE. The statistical significance of differences in mean values was assessed by Student's *t*-test. Differences where $P < 0.05$ were considered significant. Statistical analyses were performed using Statcel2 (OMS, Saitama, Japan).

RESULTS

Glucose metabolism and insulin secretion in RIP-GG Tg mice treated with STZ. When RIP-GG Tg mice and their non-Tg littermates were fed a diet of MCTD and treated with STZ, blood glucose levels were significantly elevated in both groups at 7 and 14 days posttreatment compared with vehicle-treated mice (Fig. 1*A*), and body weights were significantly decreased in both groups at 7 and 14 days posttreatment compared with vehicle-treated mice (Fig. 1*B*). At 14 days posttreatment, serum insulin levels were significantly decreased in STZ-treated mice, and when compared between genotypes, the insulin levels were significantly higher in RIP-GG Tg mice than in non-Tg littermates (Fig. 1*D*), although only the tendency was observed at 7 days posttreatment (Fig. 1*C*). The glucose levels in RIP-GG Tg mice, however, were not improved even at 14 days post treatment (Fig. 1*A*).

Insulin mRNA expression and β-cell numbers in RIP-GG Tg mice treated with STZ. The pancreatic insulin 1 and PDX-1 mRNA levels were not changed in RIP-GG Tg mice 7 days after STZ treatment but were significantly elevated in RIP-GG Tg mice 14 days after STZ treatment, with increased tendency in pancreatic insulin contents (Fig. 2, *A, B, E*). Pancreatic ghrelin mRNA levels were increased ~70-fold in RIP-GG Tg mice compared with their non-Tg littermates (Fig. 2*C*). The pancreatic GHS-R mRNA levels were not changed with STZ treatment and were not different between the genotypes (Fig. 2*D*). We assessed β-cell numbers in the islets of RIP-GG Tg mice 7 and 14 days after STZ treatment (Fig. 3). In accord with the insulin mRNA levels, the ratio of insulin$^+$ cell area per islet was significantly higher in RIP-GG Tg mice than in their non-Tg littermates 14 days after STZ treatment (Fig. 3, *D* and *E*), although the restoration of β-cell area was limited, considering the fact that the β-cell area in vehicle-treated RIP-GG Tg mouse was 83.7 ± 0.67% and that of their non-Tg littermates was 82.9 ± 0.74% (Fig. 3*G*). And the difference was not observed without STZ treatment (β-cell areas on *day 0*: RIP-GG Tg vs. non-Tg: 88.9 ± 0.71 vs. 87.6 ± 0.99%, $P = 0.29$), as reported previously (2). The number of insulin$^+$ cells per islet was also significantly higher in RIP-GG Tg mice than in vehicle-treated control animals 14 days after STZ treatment (Fig. 3*F*). These differences were not observed 7 days after STZ treatment (Fig. 3, *A–C*).

Phospho-histone H3$^+$/insulin$^+$ cells and Ki67$^+$/insulin$^+$ cells in RIP-GG Tg mice treated with STZ. To determine whether the increased number of insulin$^+$ cells in the islets of RIP-GG Tg mice was due to increased β-cell proliferation, we assessed phospho-histone H3 and Ki67 expression, which indicate proliferating cells, in the islets of RIP-GG Tg mice 7 and 14 days after STZ treatment. The ratios of phospho-histone H3$^+$/insulin$^+$ cells or Ki67$^+$/insulin$^+$ cells to insulin$^+$ cells were not changed in RIP-GG Tg mice 7 days after STZ treatment (Fig. 4, *A–D*) but were significantly higher in the islets of RIP-GG Tg mice 14 days after STZ treatment (Fig. 4, *E–H*), indicating that β-cell proliferation had increased in these animals at 14 days posttreatment.

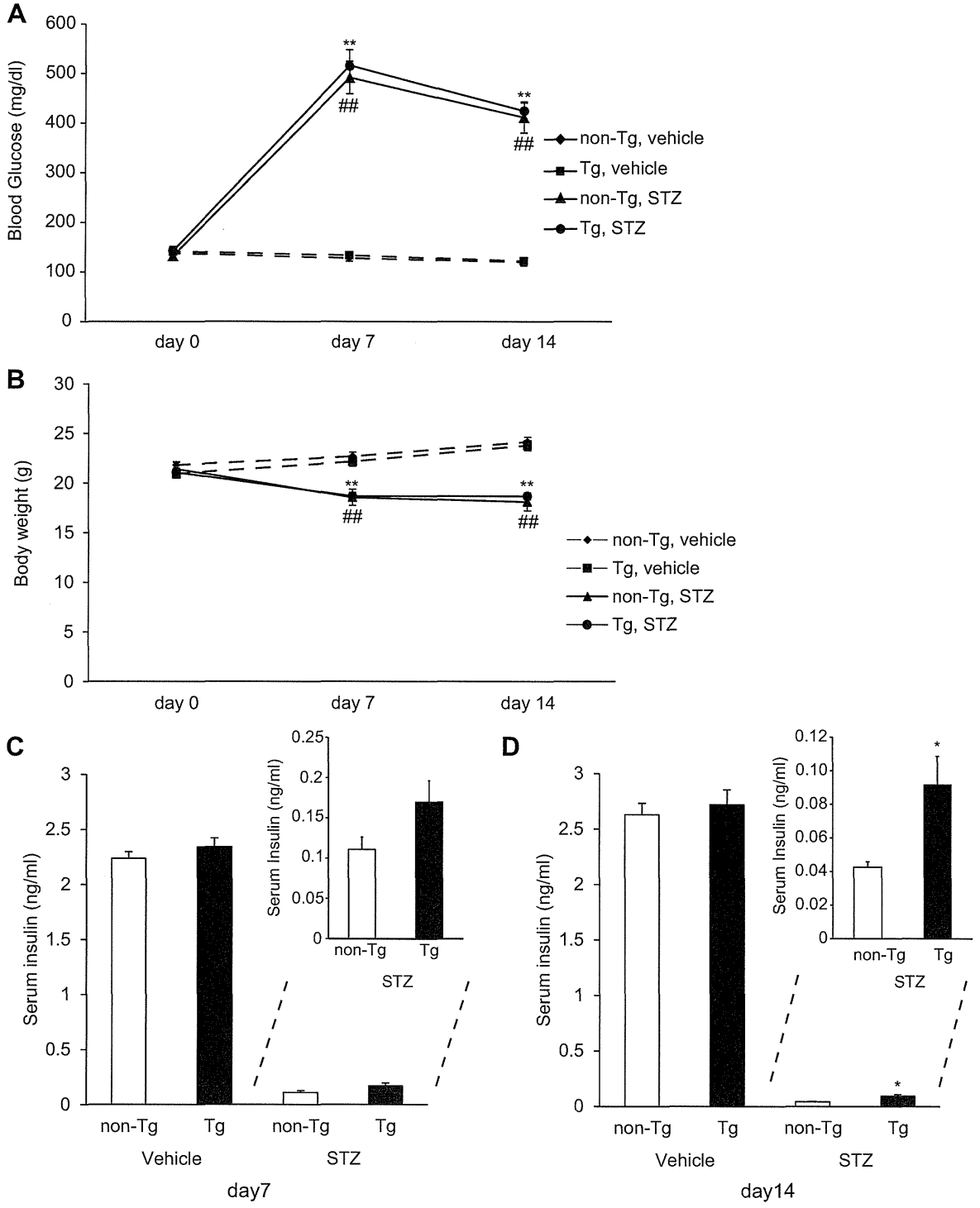

Fig. 1. Serum insulin levels are increased in STZ-treated RIP-GG Tg (rat insulin II promoter-ghrelin internal ribosomal sequence ghrelin *O*-acyltransferase transgenic) mice compared with control animals. *A* and *B*: blood glucose levels (*A*) and body weight (*B*) in RIP-GG transgenic mice (Tg) and their non-Tg littermates treated with STZ or vehicle alone; $n = 8$–10. **,##$P < 0.01$ vs. vehicle alone. *C* and *D*:s insulin levels in Tg mice and their non-Tg littermates treated with STZ or vehicle 7 days (*C*) or 14 days posttreatment (*D*); $n = 8$–10. *$P < 0.05$.

Short-term effects of STZ treatment: residual β-cell numbers and apoptotic index in islets of RIP-GG tg mice. Finally, we attempted to elucidate whether overexpressed ghrelin had direct protective effects on β-cells against STZ treatment. Since we could not detect any TUNEL-positive cells or cleaved caspase-3-positive cells in the islets 14 days after STZ treatment (data not shown), we examined residual β-cells and the apoptotic index in islets of RIP-GG Tg mice soon after STZ administration. One day postadministration of the drug, cell nuclei in the islet core were diminished; however, strong immunoreactivity for insulin was still broadly observed, probably due to leakage of insulin from damaged β-cells (Fig. 5*A*).

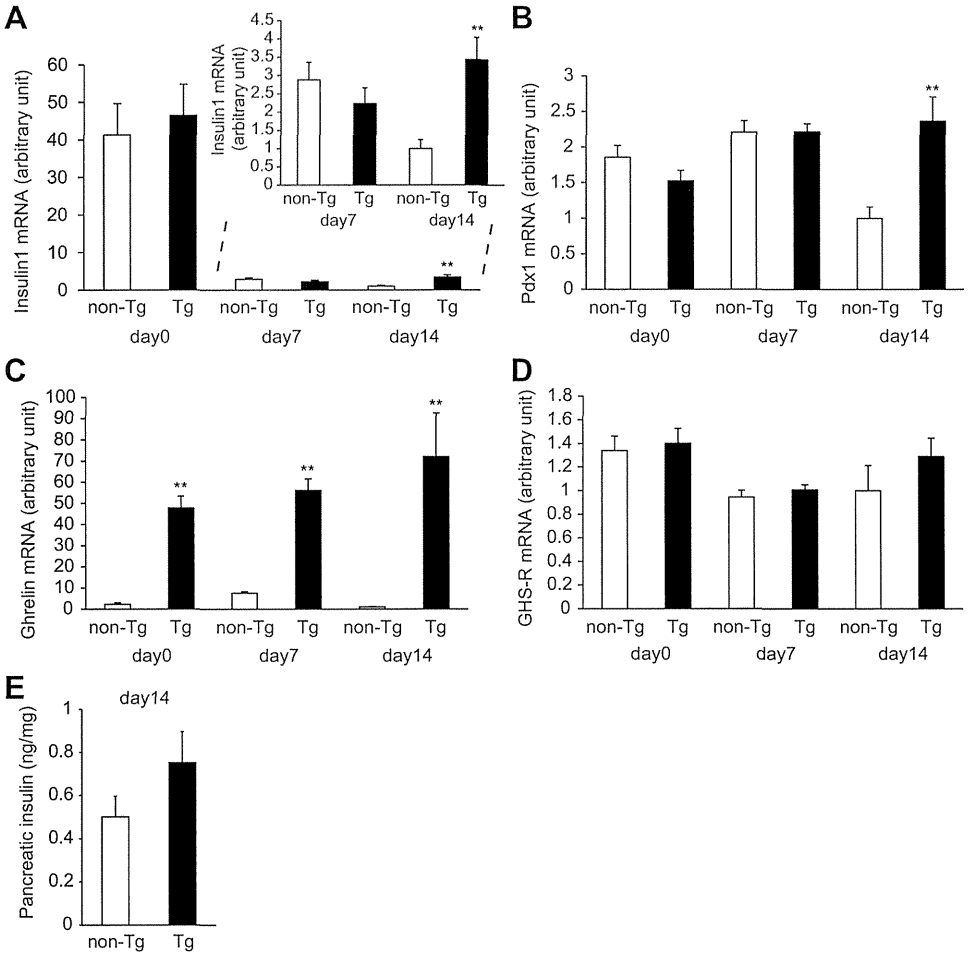

Fig. 2. Pancreatic insulin and Pdx-1 mRNA levels are increased in STZ-treated RIP-GG Tg mice compared with controls. Pancreatic insulin 1 (*A*), Pdx-1 (*B*), ghrelin (*C*), and GHS-R (*D*) mRNA levels in RIP-GG Tg mice (Tg) and their non-Tg littermates 0, 7, and 14 days post-STZ treatment; $n = 7$–10. At *day 14*, pancreatic insulin 1, Pdx-1, and ghrelin mRNA levels were significantly higher in Tg compared with their non-Tg littermates. $^{**}P < 0.01$. *E*: pancreatic insulin concentration in Tg and non-Tg littermates 14 days post-STZ treatment; $n = 7$.

This artifact made it difficult to accurately determine the number of residual β-cells. As an alternative, we assessed insulin mRNA levels in the pancreas of RIP-GG Tg mice before and 1 day after treatment. The pancreatic insulin mRNA levels were significantly decreased in both groups 1 day post-treatment, and there was no difference in insulin mRNA levels between the genotypes, indicating that β-cell destruction by STZ was not affected by overexpressed ghrelin (Fig. 5*B*). In addition, to determine whether the apoptotic cells were increased, we assessed TUNEL and cleaved caspase-3 expression in islets from RIP-GG Tg mice. The ratio of TUNEL$^+$ cell or cleaved caspase-3$^+$ cell number per islets area was not significantly different from that of their non-Tg littermates (Fig. 5, *C–F*).

DISCUSSION

In this study, we found that overexpression of intraislet ghrelin ameliorated insulin secretion in an STZ-induced diabetic mouse model by stimulating the proliferation of β-cells in the islets. This finding is in accord with our previous reports that exogenous ghrelin administration stimulates β-cell proliferation in STZ-treated neonate rats (13). In the previous study, it was not clear whether the stimulatory effects of ghrelin on β-cells were direct or indirect. We hypothesized that indirect mechanisms could be mediated through ghrelin's GH-stimulating and/or orexigenic properties. Here, by using RIP-GG Tg mice, in which intraislet ghrelin levels are elevated without major changes in plasma ghrelin levels (2), we clearly demonstrated that ghrelin directly stimulated β-cell proliferation in vivo after STZ treatment.

Although serum insulin levels were elevated in STZ-treated RIP-GG Tg mice, glucose levels were not improved to the degree observed in ghrelin-treated neonate STZ rats (13). The relatively weak effect observed in this study may have been due to the differences in age and species compared with the previous study. In rats, β-cell numbers continue to increase after birth and reach a steady-state level at weaning (10). Accordingly, in the neonate STZ-treated rat model, β-cell numbers recover to some degree even without any therapeutic treatment, and elevated glucose levels temporally return to normal for several weeks after STZ administration (30). Here, we used adult mice with limited capacity for β-cell proliferation (10). Since RIP-GG Tg mice must be fed MCTD in order to increase islet ghrelin levels, we could not study the mice before weaning. The age-related differences in β-cell proliferative capacities may explain the disparities in the intensity of ghrelin activity between the current study and the previous report. Another possibility is that the differences reflect species-specific variations. β-Cell sensitivity to STZ is known to be different among species (31). For example, rats are more sensitive than mice to the effects of the drug (31). This difference in STZ sensitivity may have affected the results of

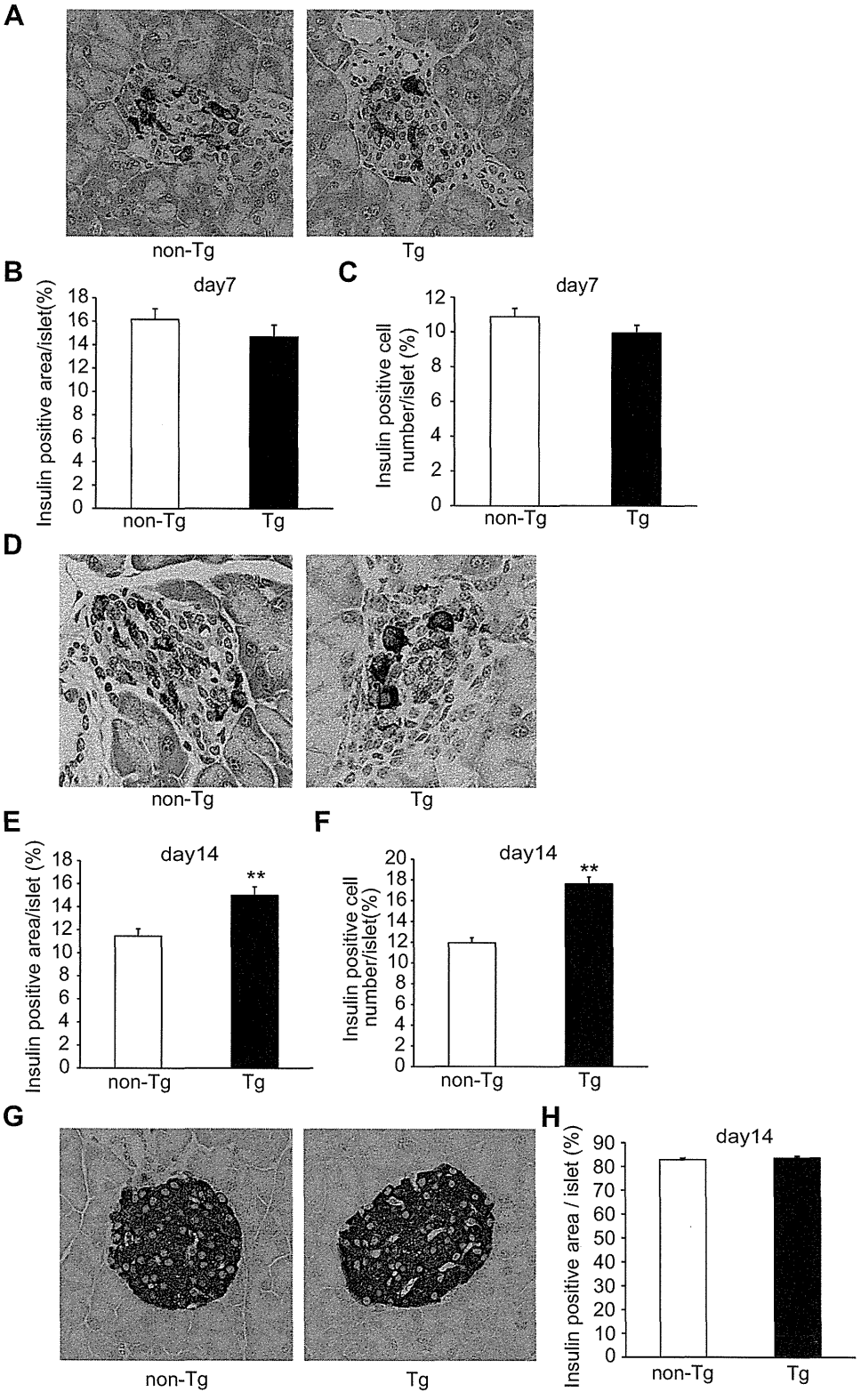

Fig. 3. Compared with control animals, RIP-GG Tg mice have more insulin$^+$ islet cells after STZ treatment. A in islets 14 days post-STZ treatment were significantly higher in RIP-GG Tg mice than in their non-Tg littermates. *A* and *D*: representative images of tissue sections from Tg and non-Tg islets 7 days (*A*) and 14 days post-STZ treatment (*D*) reacted with an anti-insulin antibody. *B* and *E*: ratio of the area occupied by insulin$^+$ cells to the area of the entire islet 7 days (*B*) and 14 days post-STZ treatment (*E*). *C* and *F*: number of insulin$^+$ cells in islets of RIP-GG Tg mice 7 days (*C*) and 14 days post-STZ treatment (*F*); $n = 7–8$. $^{**}P < 0.01$. *G*: representative images of tissue sections from Tg and non-Tg islets 14 days post-vehicle treatment. *H*: ratio of the area occupied by insulin$^+$ cells to the area of the entire islet 14 days post-vehicle treatment; $n = 7$.

these studies. Age and species differences aside, we cannot completely rule out the possibility that exogenously administered ghrelin may have exhibited both direct and indirect effects on β-cells in the neonate rat STZ model. At least the current levels of overexpression of ghrelin in the islets seemed not to have enough power to improve the glucose tolerance in adult STZ mouse model.

Ghrelin is reported to stimulate the proliferation of several cell lines, including the pancreatic cancer cell line PANC1 (9), the somatotroph cell line GH3 (21), the prostate cancer cell line

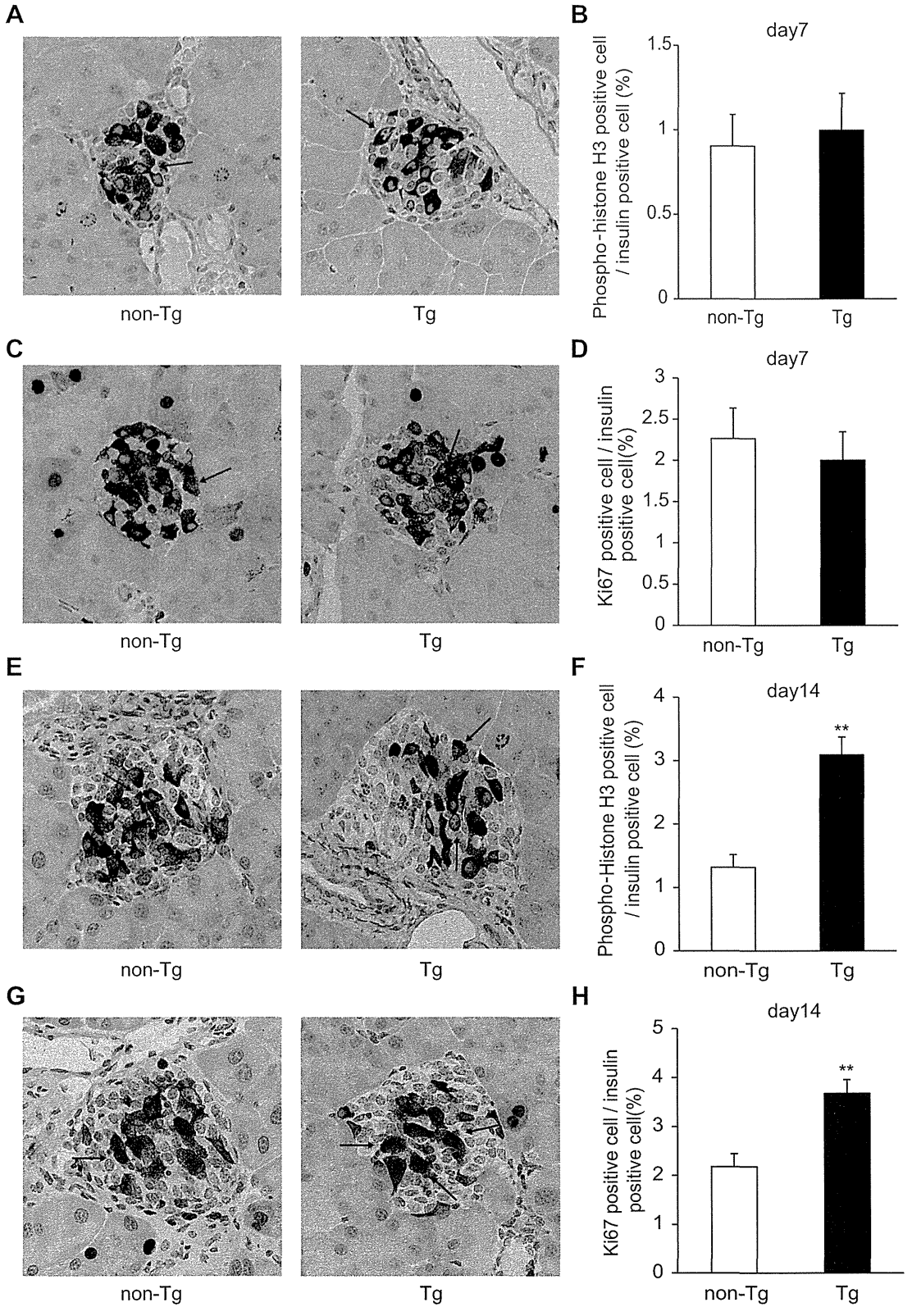

Fig. 4. Phospho-histone H3$^+$ cells are more abundant in islets of RIP-GG Tg mice than in controls. *A* and *C*: representative images of islet tissue sections from Tg mice and their non-Tg littermates 7 days post-STZ treatment. Sections were immunostained with an anti-phospho-histone H3 antibody (*A*) or an anti-Ki67 antibody (*C*) (brown, arrow) and an anti-insulin antibody (purple). *B* and *D*: ratio of phospho-histone H3$^+$ cells (*B*) or Ki67$^+$ cells (*D*) to insulin$^+$ cells in islets of Tg mice and their non-Tg littermates 7 days post-STZ treatment; $n = 5$. *E* and *G*: representative images of islet tissue sections from Tg mice and their non-Tg littermates 14 days post-STZ treatment. Sections were immunostained with an anti-phospho-histone H3 antibody (*E*) or an anti-Ki67 antibody (*G*) (brown, arrow) and an anti-insulin antibody (purple). *F* and *H*: ratio of phospho-histone H3$^+$ cells (*F*) or Ki67$^+$ cells (*H*) to insulin$^+$ cells in islets of Tg mice and their non-Tg littermates 14 days post-STZ treatment; $n = 7–8$. $^{**}P < 0.01$.

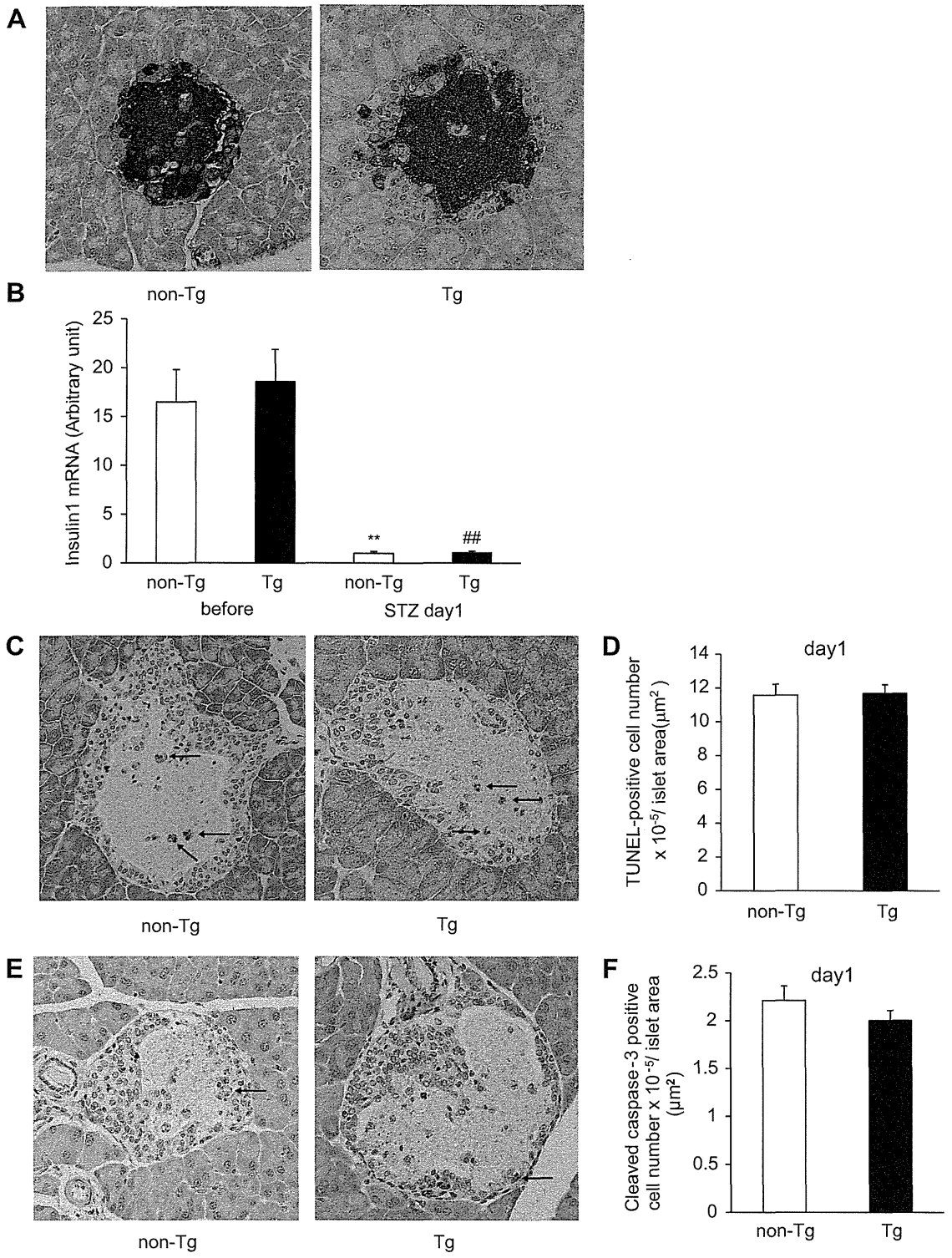

Fig. 5. No differences were observed between the residual β-cell populations and the apoptotic indexes in islets of STZ-treated RIP-GG Tg and control mice. *A*: representative images of islet tissue sections from Tg mice and their non-Tg littermates. One day post-STZ treatment, sections were stained with an anti-insulin antibody (brown). *B*: pancreatic insulin 1 mRNA levels observed in Tg mice and their non-Tg littermates before or 1 day post-STZ treatment; $n = 11$–12. **,##$P <$ 0.01 vs. before. *C* and *E*: Representative images of tissue sections from Tg and non-Tg islets 1 day post-STZ treatment reacted with TUNEL reagents (*C*) or an anti-cleaved caspase-3 antibody (*E*). *D* and *F*: number of TUNEL$^+$ cells (*D*) or cleaved caspase-3$^+$ cells (*F*) in islet cores did not differ between RIP-GG Tg mice and non-Tg controls; $n = 5$.

PC3 (15), and osteoblasts (19). Conversely, the peptide has been observed to inhibit the growth of tumors and tumor-derived cell lines including human breast carcinoma (6) and fetal thyroid and thyroid follicular tumors (28). Thus, our results are in accord with previous reports that ghrelin can stimulate cell proliferation. Given that β-cell proliferation is not increased at a basal state in RIP-GG Tg mice (2), the proliferative effects of ghrelin on β-cells seem to be limited. β-Cell proliferation is enhanced in STZ- (30) or alloxan-treated rodents (29) in a partially pancreatectomized rat (4) and in a ductally ligated hamster (23). However, the mechanisms underlying the stimulation of β-cell proliferation in these injury models have not yet been completely elucidated. Ghrelin may synergize with these injury-derived proliferative effects on β-cells. Further studies will be needed to clarify the precise mechanisms by which ghrelin stimulates β-cell proliferation.

Several lines of evidence suggest that ghrelin can exhibit antiapoptotic effects on a variety of cell types (1, 7, 12, 16, 17). With respect to β-cells, Granata et al. (12) reported that ghrelin prevented apoptosis in the β-cell lines HIT-T15 and INS-1E, as well as in human islets. By contrast, in this study we could not detect differences in the apoptotic index of the islets between RIP-GG Tg and control mice. The discrepancy between the previous results and this study may be due to differences in experimental conditions. For example, Granata et al. used β-cell lines and isolated islets in vitro and induced apoptosis by serum starvation or the addition of interferons (12), whereas we used an in vivo STZ-induced diabetic mouse model. Furthermore, it has been reported that low doses of STZ induce β-cell apoptosis, whereas high doses cause β-cell necrosis (24). In this study, we used 100 mg/kg, which is a relatively high dose. Therefore, although we detected very few apoptotic cells in RIP-GG Tg islets, on the basis of these results we cannot determine whether ghrelin directly protected β-cells from apoptosis.

The results of this study indicate that introduction of ghrelin and GOAT to β-cells may have beneficial effects on diabetes in the sense that it may increase β-cell mass. On the other hand, previous reports indicate that exogenous ghrelin administration suppresses insulin secretion and elevates blood glucose level and that inhibition of ghrelin or GOAT ameliorates glucose tolerance in mice by enhancing insulin secretion (3, 26, 32). Considering that RIP-GG Tg mice have normal glucose tolerance and insulin secretion, the level of ghrelin needed to stimulate β-cell proliferation after STZ-induced β-cell injury seems to be lower than the level to suppress insulin secretion. It would be necessary to keep in mind the deleterious side of ghrelin's effect on β-cells when therapeutic application of ghrelin on β-cell injury is considered.

One drawback of this study is that ghrelin may be produced in tissues other than the β-cell, such as hypothalamus, as is the case in the RIP-Cre mice (8), which may have affected β-cell proliferation. Actually, the mRNA levels of ghrelin and GOAT were elevated in the hypothalamus of RIP-GG Tg mice (2). However, when we examined the expression of the peptide by immunohistochemistry, we found no apparent differences of the ghrelin-like immunoreactivities in the hypothalamus between Tg mice and controls (data not shown). Furthermore, there were no differences in body weight between two groups. Therefore, we doubt that physiologically meaningful levels of ghrelin were produced in the hypothalamus of RIP-GG Tg mice. Nonetheless, we cannot completely eliminate the possibility that the leakage expression of ghrelin in other tissues may have also affected the β-cell proliferation indirectly.

In conclusion, we found that serum insulin levels, β-cell numbers and β-cell proliferation were significantly elevated in RIP-GG Tg mice after STZ treatment without amelioration in glucose levels. These results indicate that ghrelin can directly stimulate β-cell proliferation in vivo after β-cell injury even without its orexigenic or GH-stimulating activities, although it did not have enough impact to normalize the glucose tolerance in adult mice.

ACKNOWLEDGMENTS

We thank Chieko Ishimoto and Chinami Shiraiwa for excellent technical assistance.

GRANTS

This study was supported by funds from the Ministry of Education, Culture, Sports, Science and Technology of Japan and the Ministry of Health, Labor and Welfare of Japan.

DISCLOSURES

No conflicts of interest, financial or otherwise, are declared by the author(s).

AUTHOR CONTRIBUTIONS

Author contributions: M.B., H.I., and H.K. performed experiments; M.B. and H.I. analyzed data; M.B., H.I., H.A., K.H., S.A., K.N., K.K., and T.A. interpreted results of experiments; M.B. and H.I. prepared figures; M.B. and H.I. drafted manuscript; M.B., H.I., H.A., K.H., S.A., K.N., K.K., and T.A. edited and revised manuscript; H.I., K.K., and T.A. conception and design of research; H.I., K.N., K.K., and T.A. approved final version of manuscript.

REFERENCES

1. **Baldanzi G, Filigheddu N, Cutrupi S, Catapano F, Bonissoni S, Fubini A, Malan D, Baj G, Granata R, Broglio F, Papotti M, Surico N, Bussolino F, Isgaard J, Deghenghi R, Sinigaglia F, Prat M, Muccioli G, Ghigo E, Graziani A.** Ghrelin and des-acyl ghrelin inhibit cell death in cardiomyocytes and endothelial cells through ERK1/2 and PI 3-kinase/AKT. *J Cell Biol* 159: 1029–1037, 2002.
2. **Bando M, Iwakura H, Ariyasu H, Hosoda H, Yamada G, Hosoda K, Adachi S, Nakao K, Kangawa K, Akamizu T.** Transgenic overexpression of intraislet ghrelin does not affect insulin secretion or glucose metabolism in vivo. *Am J Physiol Endocrinol Metab* 302: E403–E408, 2012.
3. **Barnett BP, Hwang Y, Taylor MS, Kirchner H, Pfluger PT, Bernard V, Lin YY, Bowers EM, Mukherjee C, Song WJ, Longo PA, Leahy DJ, Hussain MA, Tschop MH, Boeke JD, Cole PA.** Glucose and weight control in mice with a designed ghrelin O-acyltransferase inhibitor. *Science* 330: 1689–1692, 2010.
4. **Bonner-Weir S, Trent DF, Weir GC.** Partial pancreatectomy in the rat and subsequent defect in glucose-induced insulin release. *J Clin Invest* 71: 1544–1553, 1983.
5. **Butler AE, Janson J, Bonner-Weir S, Ritzel R, Rizza RA, Butler PC.** Beta-cell deficit and increased beta-cell apoptosis in humans with type 2 diabetes. *Diabetes* 52: 102–110, 2003.
6. **Cassoni P, Papotti M, Ghe C, Catapano F, Sapino A, Graziani A, Deghenghi R, Reissmann T, Ghigo E, Muccioli G.** Identification, characterization, and biological activity of specific receptors for natural (ghrelin) and synthetic growth hormone secretagogues and analogs in human breast carcinomas and cell lines. *J Clin Endocrinol Metab* 86: 1738–1745, 2001.
7. **Chung H, Kim E, Lee DH, Seo S, Ju S, Lee D, Kim H, Park S.** Ghrelin inhibits apoptosis in hypothalamic neuronal cells during oxygen-glucose deprivation. *Endocrinology* 148: 148–159, 2007.
8. **Cui Y, Huang L, Elefteriou F, Yang G, Shelton JM, Giles JE, Oz OK, Pourbahrami T, Lu CY, Richardson JA, Karsenty G, Li C.** Essential role of STAT3 in body weight and glucose homeostasis. *Mol Cell Biol* 24: 258–269, 2004.

9. **Duxbury MS, Waseem T, Ito H, Robinson MK, Zinner MJ, Ashley SW, Whang EE.** Ghrelin promotes pancreatic adenocarcinoma cellular proliferation and invasiveness. *Biochem Biophys Res Commun* 309: 464–468, 2003.
10. **Finegood DT, Scaglia L, Bonner-Weir S.** Dynamics of beta-cell mass in the growing rat pancreas Estimation with a simple mathematical model. *Diabetes* 44: 249–256, 1995.
11. **Friedrichsen BN, Galsgaard ED, Nielsen JH, Moldrup A.** Growth hormone- and prolactin-induced proliferation of insulinoma cells, INS-1, depends on activation of STAT5 (signal transducer and activator of transcription 5). *Mol Endocrinol* 15: 136–148, 2001.
12. **Granata R, Settanni F, Biancone L, Trovato L, Nano R, Bertuzzi F, Destefanis S, Annunziata M, Martinetti M, Catapano F, Ghe C, Isgaard J, Papotti M, Ghigo E, Muccioli G.** Acylated and unacylated ghrelin promote proliferation and inhibit apoptosis of pancreatic beta-cells and human islets: involvement of 3′,5′-cyclic adenosine monophosphate/protein kinase A, extracellular signal-regulated kinase 1/2, and phosphatidyl inositol 3-kinase/Akt signaling. *Endocrinology* 148: 512–529, 2007.
13. **Irako T, Akamizu T, Hosoda H, Iwakura H, Ariyasu H, Tojo K, Tajima N, Kangawa K.** Ghrelin prevents development of diabetes at adult age in streptozotocin-treated newborn rats. *Diabetologia* 49: 1264–1273, 2006.
14. **Iwakura H, Hosoda K, Doi R, Komoto I, Nishimura H, Son C, Fujikura J, Tomita T, Takaya K, Ogawa Y, Hayashi T, Inoue G, Akamizu T, Hosoda H, Kojima M, Kangawa K, Imamura M, Nakao K.** Ghrelin expression in islet cell tumors: augmented expression of ghrelin in a case of glucagonoma with multiple endocrine neoplasm type I. *J Clin Endocrinol Metab* 87: 4885–4888, 2002.
15. **Jeffery PL, Herington AC, Chopin LK.** Expression and action of the growth hormone releasing peptide ghrelin and its receptor in prostate cancer cell lines. *J Endocrinol* 172: R7–R11, 2002.
16. **Kim MS, Yoon CY, Jang PG, Park YJ, Shin CS, Park HS, Ryu JW, Pak YK, Park JY, Lee KU, Kim SY, Lee HK, Kim YB, Park KS.** The mitogenic and antiapoptotic actions of ghrelin in 3T3-L1 adipocytes. *Mol Endocrinol* 18: 2291–2301, 2004.
17. **Kim SW, Her SJ, Park SJ, Kim D, Park KS, Lee HK, Han BH, Kim MS, Shin CS, Kim SY.** Ghrelin stimulates proliferation and differentiation and inhibits apoptosis in osteoblastic MC3T3-E1 cells. *Bone* 37: 359–369, 2005.
18. **Kojima M, Hosoda H, Date Y, Nakazato M, Matsuo H, Kangawa K.** Ghrelin is a growth-hormone-releasing acylated peptide from stomach. *Nature* 402: 656–660, 1999.
19. **Maccarinelli G, Sibilia V, Torsello A, Raimondo F, Pitto M, Giustina A, Netti C, Cocchi D.** Ghrelin regulates proliferation and differentiation of osteoblastic cells. *J Endocrinol* 184: 249–256, 2005.
20. **Nakazato M, Murakami N, Date Y, Kojima M, Matsuo H, Kangawa K, Matsukura S.** A role for ghrelin in the central regulation of feeding. *Nature* 409: 194–198, 2001.
21. **Nanzer AM, Khalaf S, Mozid AM, Fowkes RC, Patel MV, Burrin JM, Grossman AB, Korbonits M.** Ghrelin exerts a proliferative effect on a rat pituitary somatotroph cell line via the mitogen-activated protein kinase pathway. *Eur J Endocrinol* 151: 233–240, 2004.
22. **Nielsen JH, Linde S, Welinder BS, Billestrup N, Madsen OD.** Growth hormone is a growth factor for the differentiated pancreatic beta-cell. *Mol Endocrinol* 3: 165–173, 1989.
23. **Rosenberg L, Brown RA, Duguid WP.** A new approach to the induction of duct epithelial hyperplasia and nesidioblastosis by cellophane wrapping of the hamster pancreas. *J Surg Res* 35: 63–72, 1983.
24. **Saini KS, Thompson C, Winterford CM, Walker NI, Cameron DP.** Streptozotocin at low doses induces apoptosis and at high doses causes necrosis in a murine pancreatic beta cell line, INS-1. *Biochem Mol Biol Int* 39: 1229–1236, 1996.
25. **Shintani M, Ogawa Y, Ebihara K, Aizawa-Abe M, Miyanaga F, Takaya K, Hayashi T, Inoue G, Hosoda K, Kojima M, Kangawa K, Nakao K.** Ghrelin, an endogenous growth hormone secretagogue, is a novel orexigenic peptide that antagonizes leptin action through the activation of hypothalamic neuropeptide Y/Y1 receptor pathway. *Diabetes* 50: 227–232, 2001.
26. **Sun Y, Asnicar M, Saha PK, Chan L, Smith RG.** Ablation of ghrelin improves the diabetic but not obese phenotype of ob/ob mice. *Cell Metab* 3: 379–386, 2006.
27. **Takaya K, Ariyasu H, Kanamoto N, Iwakura H, Yoshimoto A, Harada M, Mori K, Komatsu Y, Usui T, Shimatsu A, Ogawa Y, Hosoda K, Akamizu T, Kojima M, Kangawa K, Nakao K.** Ghrelin strongly stimulates growth hormone release in humans. *J Clin Endocrinol Metab* 85: 4908–4911, 2000.
28. **Volante M, Allia E, Fulcheri E, Cassoni P, Ghigo E, Muccioli G, Papotti M.** Ghrelin in fetal thyroid and follicular tumors and cell lines: expression and effects on tumor growth. *Am J Pathol* 162: 645–654, 2003.
29. **Waguri M, Yamamoto K, Miyagawa JI, Tochino Y, Yamamori K, Kajimoto Y, Nakajima H, Watada H, Yoshiuchi I, Itoh N, Imagawa A, Namba M, Kuwajima M, Yamasaki Y, Hanafusa T, Matsuzawa Y.** Demonstration of two different processes of beta-cell regeneration in a new diabetic mouse model induced by selective perfusion of alloxan. *Diabetes* 46: 1281–1290, 1997.
30. **Wang RN, Bouwens L, Kloppel G.** Beta-cell proliferation in normal and streptozotocin-treated newborn rats: site, dynamics and capacity. *Diabetologia* 37: 1088–1096, 1994.
31. **Yang H, Wright JR Jr.** Human beta cells are exceedingly resistant to streptozotocin in vivo. *Endocrinology* 143: 2491–2495, 2002.
32. **Zhao TJ, Liang G, Li RL, Xie X, Sleeman MW, Murphy AJ, Valenzuela DM, Yancopoulos GD, Goldstein JL, Brown MS.** Ghrelin O-acyltransferase (GOAT) is essential for growth hormone-mediated survival of calorie-restricted mice. *Proc Natl Acad Sci USA* 107: 7467–7472, 2010.

Published in final edited form as:
Circ Cardiovasc Genet. 2013 December 1; 6(6): 624–633. doi:10.1161/CIRCGENETICS.113.000330.

Identification of Chemicals Inducing Cardiomyocyte Proliferation in Developmental Stage-Specific Manner with Pluripotent Stem Cells

Hideki Uosaki, MD, PhD[1], **Ajit Magadum, PhD**[2], **Kinya Seo, PhD**[1], **Hiroyuki Fukushima, MS**[3,4], **Ayako Takeuchi, PhD**[5], **Yasuaki Nakagawa, MD, PhD**[6], **Kara White Moyes, PhD**[7], **Genta Narazaki, PhD**[3,4], **Koichiro Kuwahara, MD, PhD**[6], **Michael Laflamme, MD, PhD**[7], **Satoshi Matsuoka, MD, PhD**[5], **Norio Nakatsuji, PhD**[8], **Kazuwa Nakao, MD, PhD**[6], **Chulan Kwon, PhD**[1], **David A. Kass, MD**[1], **Felix B. Engel, PhD**[2], and **Jun K. Yamashita, MD, PhD**[3,4]

[1]Division of Cardiology, The Johns Hopkins University School of Medicine, Baltimore, MD

[2]Experimental Renal & Cardiovascular Research, Dept of Nephropathology, Institute of Pathology, University of Erlangen-Nürnberg, Erlangen, Germany

[3]Laboratory of Stem Cell Differentiation, Stem Cell Research Center, Institute for Frontier Medical Sciences, Kyoto University, Kyoto

[4]Dept of Cell Growth & Differentiation, Center for iPS Cell Research & Application, Kyoto University, Kyoto

[5]Dept of Integrative Physiology, Faculty of Medical Sciences, University of Fukui, Fukui

[6]Dept of Medicine & Clinical Science, Kyoto University Graduate School of Medicine, Kyoto, Japan

[7]Dept of Pathology, Center for Cardiovascular Biology, University of Washington, Seattle, WA

[8]Dept of Development & Differentiation, Institute for Frontier Medical Sciences, Kyoto University, Kyoto

Abstract

Background—The proliferation of cardiomyocytes is highly restricted after postnatal maturation, limiting heart regeneration. Elucidation of the regulatory machineries for the proliferation and growth arrest of cardiomyocytes is imperative. Chemical biology is efficient to dissect molecular mechanisms of various cellular events and often provide therapeutic potentials. We have been investigating cardiovascular differentiation with pluripotent stem cells (PSCs). The combination of stem cell and chemical biology can provide novel approaches to investigate the molecular mechanisms and manipulation of cardiomyocyte proliferation.

Methods and Results—To identify chemicals that regulate cardiomyocyte proliferation, we performed a screening of a defined chemical library based on proliferation of mouse PSC-derived cardiomyocytes and identified 4 chemical compound groups - inhibitors of glycogen synthase kinase-3 (GSK3), p38 mitogen-activated protein kinase (MAPK) and Ca^{2+}/calmodulin-dependent protein kinase II (CaMKII), and activators of extracellular signal-regulated kinase (ERK). Several

Correspondence: Hideki Uosaki, MD, PhD, Division of Cardiology, The Johns Hopkins University, School of Medicine, 720 Rutland Ave. Ross 954, Baltimore, MD 21218, Tel: +1-410-512-2154, Fax: +1-410-502-2558, huosaki1@jhmi.edu. Jun K. Yamashita, MD, PhD, Laboratory of Stem Cell Differentiation, Institute for Frontier Medical Sciences, Kyoto University, 53, Shogoin Kawaharacho, Sakyo-ku, Kyoto, 606-8507, Japan, Tel: +81-75-751-3853, Fax: +81-75-751-4824, juny@frontier.kyoto-u.ac.jp.

Conflict of Interest Disclosures: None.

appropriate combinations of chemicals synergistically enhanced proliferation of cardiomyocytes derived from both mouse and human PSCs, notably up to a 14-fold increase in mouse cardiomyocytes. We also examined the effects of identified chemicals on cardiomyocytes in various developmental stages and species. Whereas ERK activators and CaMKII inhibitors showed proliferative effects only on cardiomyocytes in early developmental stages, GSK3 and p38 MAPK inhibitors substantially and synergistically induced reentry and progression of cell cycle in not only neonatal but also adult cardiomyocytes.

Conclusions—Our approach successfully uncovered novel molecular targets and mechanisms controlling cardiomyocyte proliferation in distinct developmental stages and offered PSC-derived cardiomyocytes as a potent tool to explore chemical-based cardiac regenerative strategies.

Keywords

cardiomyocyte; embryonic stem cell; proliferation; small molecules

Life-threatening heart diseases, such as myocardial infarction and heart failure, are major causes of death in developed countries. Due to the almost non-existent cardiomyocyte turnover in the human heart after birth, recovery of cardiac function after heart disease is insufficient.[1–3] The low levels of proliferation and regeneration ability of cardiomyocytes must be overcome to effectively treat these diseases. Although numerous causes of postnatal cell cycle arrest were extensively investigated, such as balances of cyclins, cyclin dependent kinases (CDKs) and CDK inhibitors[4], growth factors[5–9], transcription factors[10–14] and micro RNA[15], heart regenerative medicine has not been effective. One of the limitations is lack of efficient methods for manipulating multiple factors simultaneously.

We hypothesized that a chemical biological approach would be a suitable answer to this problem. Compared to conventional genetic methods, chemical-biological approaches for exploring key biological mechanisms have many advantages, enabling temporal control, rapid inhibition or activation, and regulation of functionally overlapping targets.[16,17] Moreover, chemicals can function across similar species and can be directly applied as therapeutic drugs. Thus, identifying novel chemicals would be an efficient approach to elucidate novel mechanisms regulating cardiomyocyte proliferation and finally employ cardiac regeneration as a therapeutic strategy. Nevertheless, no efficient chemical screening platform for cardiomyocyte proliferation has been explored to date. Recent advances in imaging and analyzing have led to novel approaches to analyze numerous samples automatically. These cell-based and imaging-based methods to screen are called high-content screening (HCS), providing various information on cellular phenotype including cell division.[18]

Pluripotent stem cells (PSCs), including both embryonic stem cells (ESCs) and induced pluripotent stem cells (iPSCs) have great potentials for therapeutic purpose and for drug discovery as they can give rise to any cell types, including cardiomyocytes.[19–23] We have been investigating cardiovascular cell differentiation and regeneration with the use of PSCs, and have established efficient methods for cardiac differentiation from mouse and human PSCs.[24–28] Here we combined our stem cell technology and chemical-biology with HCS to identify chemicals inducing cardiomyocyte proliferation. We successfully identified several chemicals with distinct molecular targets and confirmed their proliferative effects on cardiomyocytes from mouse PSCs. We further demonstrated that the chemical-induced effects on cardiomyocytes from different stages of maturation - embryos, neonates and adults. This study provides novel understanding for molecular machineries and would offer efficient ways to regulate cardiomyocyte proliferation with chemicals.

Methods

Reagents and Antibodies

The SCADS inhibitor kit containing approximately 280 well-established kinase inhibitors[29,30] was a gift from the Screening Committee of Anticancer Drugs supported by a Grant-in-Aid for Scientific Research on Priority Area 'Cancer' from The Ministry of Education, Culture, Sports, Science and Technology, Japan. See Supplemental Methods for reagents and antibodies.

High-Content Screening

The screening process is summarized in Figure S1 and S2. FACS-purified mouse ESC-derived cardiomyocytes (mESCMs) were plated on 0.1% gelatin-coated 96-well plates at 500 cells per well. Cells were treated with chemicals from SCADS inhibitor kit (0.2μM–5μM) for 5 days, followed by fixation and staining with anti-α-myosin heavy chain (αMHC) antibody and DAPI. A DAPI-positive spot in an αMHC-positive area was counted as one nucleus (Figure S2c). αMHC-positive nuclei in four low magnification fields, covering approximately 60% of a single well of 96-well plates, were counted using HCS system ImageXpress (Molecular Devices, Sunnyvale, CA, USA) and image processing software MetaXpress (Molecular Devices).

Statistics

All experiments were repeated at least three times, except the first screen that was repeated twice. Values were reported as mean ± SD and were analyzed by Mann-Whitney test (for two-group comparison), or by Dunn's test (for multiple comparison) using a statistics software, GraphPad Prism (GraphPad Software, Inc., CA, USA). Values of $p < 0.05$ were considered to be statistically significant.

See Supplemental Methods for mouse ESC and human ESC/iPSC culture and differentiation, cardiomyocyte isolation, immunostaining, cell-cycle analysis by flow cytometry, Western blotting, gene knockdown, electrophysiological study, and quantitative reverse transcriptional polymerase chain reaction (qPCR).

Results

Chemical Library Screening for Cardiomyocyte Proliferation in mESCMs

A mouse ESC line carrying αMHC promoter-driven enhanced green fluorescent protein (αMHC-EGFP)[25] was used to prepare purified early differentiated cardiomyocytes (Figure S1), with which we evaluated the chemical-induced effects on cardiomyocyte proliferation. mESCMs appear at 3–4 days after Flk1-positive mesoderm cells were cultured on OP9 stroma cells as we previously reported (Flkd3 to d4; Figure S1).[25,27] Within a few days after the cells differentiated to cardiomyocytes, they ceased their proliferation similar to cardiomyocytes *in vivo*. To screen chemicals that exhibit a direct pro-proliferative effect on mESCMs, we sorted, purified and re-cultured αMHC-EGFP-positive mESCMs at Flkd6 (Figure S2b–d). For the primary screen, we performed HCS to directly count the number of cardiomyocyte nuclei (Figure S2c). Purified mESCMs were re-plated on 96-well plate with treatment of each chemical from the SCADS inhibitor kit in three concentrations (0.2, 1, 5 μM). Five days after treatment (Flkd6+5), the average number of mESCM nuclei was 35.6 ± 17.5 (cells per field, n = 35) in the control condition. Seven chemicals increased mESCM nucleus number more than mean + 2SD of control (red spots in Figure 1a and Table S1). Two Ca^{2+}/calmodulin-dependent kinase II (CaMKII) inhibitors increased the number of mESCM nuclei more than mean + 1SD of control (blue spots in Figure 1a and Table S1).

Because more than 80% of murine mature cardiomyocytes in adults are reported to have two nuclei[1, 31], an increase in the number of cardiomyocyte nuclei may not directly reflect the actual increase in the number of cardiomyocytes. To evaluate the effects of the chemicals on the actual cardiomyocyte number, we performed a secondary screen with seven small molecules of independent kinase targets among the nine candidate chemicals (Table S1). We purified mESCMs, re-cultured with chemicals for 5 days, and calculated the actual cardiomyocyte number by cell counting and flow cytometry for αMHC-EGFP (Figure S2d). Three out of the seven chemicals significantly increased mESCM cell number (Figure 1b). BIO (GSK3 inhibitor, 1 μM), SU1498 (Flk1 inhibitor, 5 μM), and KN93 (CaMKII inhibitor, 5 μM) increased cardiomyocyte number to 3.4 ± 1.4, 2.5 ± 0.6, and 2.2 ± 0.4 times over control, respectively.

Next, we compared mESCM number between Flkd6+2 and Flkd6+5 to confirm whether these chemicals could actually increase cardiomyocyte proliferation and whether they did not simply improve the re-plating viability of mESCMs. Whereas re-plated mESCMs showed no increase in cell number with DMSO alone, all three chemicals significantly increased mESCM number during Flkd6+2 to Flkd6+5 (Figure 1c). We further confirmed cardiomyocyte proliferation with time-lapse video recording (Figure 1d, Supplemental Movie 1–4). Whereas a control cardiomyocyte (Movie S1) ceased proliferation and just underwent hypertrophic change, cardiomyocytes treated with these chemicals caused cell division and proliferation (Movie S2–4). These data clearly show that the three chemicals (BIO, SU1498 and KN93) enhance mESCM proliferation and increase in mESCM number accompanying actual cell division but not binucleation.

Induction of Cell Cycle Progression in Cardiomyocytes by Chemicals

Next, we examined changes in mESCM cell cycle. The ratio of S phase in mESCMs, as estimated with 3 hour pulse-labeled EdU incorporation, and the ratio of M phase in mESCMs, as estimated by immunostaining of Phosphorylated Histone H3 (pH3) at Flkd6+3 were increased more than 2.2 times by BIO treatment and increased approximately 1.5–2 times by SU1498 and KN93 (Figure 2a–c). The ratio of 4N cardiomyocytes was examined as doubled DNA contents (4N) and EdU-negative cells in cardiac Troponin T (cTnT)-positive population by flow cytometry. 4N cardiomyocytes, consisting of cells in G2/M phase and cells with binuclei, were not increased by any of chemical treatment but reduced by KN93 treatment compared with DMSO treatment, suggesting binuclear cardiomyocytes were not induced by these chemicals (Figure 2d). Western blotting for cyclins showed that BIO but not SU1498 or KN93 treatment increased Cyclin D2 and Cyclin D3 (Figure 2e) as reported.[32] On the other hand, a CDK inhibitor, *Ink4b* expression was downregulated 30% by treatment of each chemical at Flkd6+2 (Figure 2f). Downregulation of *Ink4b* was sustained until Flkd6+5 in SU1498 or KN93 treatment (Figure 2g). These results indicate that these chemicals actually induce cell cycle progression in cardiomyocytes by regulating Cyclin/CDK activity.

Molecular Targets of the Chemicals

Next we confirmed the molecular targets of these three chemicals. Addition of CHIR99021, another GSK3-specific inhibitor (Figure 3a), or Wnt3a (data not shown) increased cardiomyocyte numbers similar to BIO, indicating that inhibition of GSK3 enhanced mESCM proliferation as reported in rat cardiomyocytes.[32]

SU1498, first reported as a tyrosine kinase inhibitor of vascular endothelial growth factor receptor 2 (VEGFR2; also designated as Flk1)[33], enhanced cardiomyocyte proliferation even though Flk1 is not expressed in mESCMs[25], suggesting that SU1498 exerted its effect through targets other than Flk1. SU1498 was reported to cause accumulation of